BILINGUAL PUBLISHING GROUP

Journal of Atmospheric Science Research

https://journals.bilpubgroup.com/index.php/jasr/index

REVIEW

Convective Phenomenes in the Context of Meso-β-scale Convective Structures

***Livshits E.M.*[1*], *Petrov V.I.*[2]**

[1] *Independent researcher, Frankfurt am Main, 60326, Germany.*

[2] *Independent researcher, Stafford, ST17 9XX, UK.*

ABSTRACT

This review article presents the results of radar studies of convective phenomena in Moldavia and the North Caucasus using Eulerian (ECS) and Lagrangian (LCS) coordinate systems. Application of the Lagrangian approach allowed us to exclude the influence of the tropospheric displacement and to obtain integral grid patterns of thunderstorm-hail processes. These structures are especially well manifested at small wind shears (up to 1 m/sec/km). At large shears, the mesh structures are transformed predominantly into linear structures. The methodology for obtaining integral pictures of radio echoes of thunderstorm processes is described. Intersections of linear elements, which we call facets, occur at nodes. The latter plays a particularly important role in the dynamics and kinematics of convective storms. The development of storms occurs along the facets and at the nodes of meso-β-scale convective structures (MMCS), which explains the mechanisms of splitting and merging of storms: in the first case the facets diverge, in the second case they converge. The relations of motion vectors for different types of storms are obtained. It is shown that the direction of the radio echo canopy coincides with the storm motion trajectory; the evolution vector (propagation) for the most powerful storms deviates from the storm displacement direction by 80°–135°. The structure of the updated band within which the Flanking Line is formed for supercells and multicells is studied. Mnemonic rules have been derived that allow one to infer from instantaneous patterns of anvil orientation and the mutual location of storms whether they are converging or diverging, and to identify left- or right-moving storms. A hypothesis on the internal structure of the cold front of the 2nd kind is stated. The main conclusion of the work is that the evolution of storms is determined by the configuration of meso-β-scale convective structures. This explains various convective phenomena from unified positions. The results are applicable in works on modification of convective cloudiness, for ultra-short-term forecasts of dangerous phenomena, storm warnings of the population, rescue services, etc.

Keywords: Convective storm; Motion vectors and their relations; Storm merging and splitting; Meso-β-scale convective structures; Feeder cells; Flanking Line

*CORRESPONDING AUTHOR:

Livshits E.M., Independent researcher, Frankfurt am Main, 60326, Germany; Email: evmaleposoru@googlemail.com

ARTICLE INFO

Received: 29 February 2024 | Revised: 28 April 2024 | Accepted: 8 May 2024 | Published Online: 31 May 2024

DOI: https://doi.org/10.30564/jasr.v7i3.6278

CITATION

Livshits, E.M, Petrov, V.I., 2024. Convective Phenomenes in the Context of Meso-β-scale Convective Structures. Journal of Atmospheric Science Research. 7(3): 1–38. DOI: https://doi.org/10.30564/jasr.v7i3.6278

1. Introduction

The development of convective storm fields can be visualised as a continuous process of emergence, growth, dissipation, merging or splitting. The trajectories of storms moving with different velocities and constituting an integral radar picture are not parallel to each other and experience fractures, often crossing. All these processes occur in the moving atmosphere. To the complex microphysics of cloud particles, the entanglement of flows within clouds and wind structure in the outer troposphere, and the varied kinematics of storms, one adds the influence of various convective scales. Each of these problems, complex in itself, appears in the aggregate to be almost intractable. Therefore, for an unsophisticated observer located in the Eulerian Coordinate System (ESC), all this variety of convective phenomena may cause a feeling of chaos.

To eliminate the tropospheric displacement factor, we used the Lagrangian principle. Its essence, for troposphere, is that by placing the centre of the Lagrangian Coordinate System (LCS) at the centre of the convective cell, the observer moves with it along the leading flow. This makes it possible to follow the internal dynamics of convective storms and convective storm fields in general [1]. Methodologically, such an operation consists of moving the LCS centre along a trajectory with the velocity of the leading flow, but in the opposite direction to the leading flow [2]. All radar survey files are sequentially mapped onto a single field. In this way, an integral picture (IP) of the entire thunderstorm process (TSP) or its fragment is obtained in the form of radio echo increments from one file to the next. The IP consists of both currently existing radio echoes and precipitation traces from destroyed radio echoes. Technically, this is implemented as a Lagrangian procedure (LP) in the Automated Control System—ACS MRL5 [3].

Before going on, let us give some basic definitions of the terms we use in this paper.

Convective Cell—a deep, moist, convectively induced local maximum in precipitation density that undergoes a life cycle of growth, maximum development and decline; the ascending branch of the maximal reflectivity Z indicates upward flow, and the later descending part indicates precipitation; cells in convective storms "live" from 20 to 30 minutes ("traces" of destroyed cells are radar traced much longer); the radar image of a cell is a Radar Cell (RC).

A **Radar Cell (RC)** is a single-cell cloud or part of a multi-cell cloud whose radar image displays a convectively induced local precipitation maximum in the stages of nucleation, growth, or dissipation; it is represented by a quasi-vertical and quasi-symmetric closed structure of Z reflectivity isocontours; an individual top of Z isocontours corresponds to each individual upward or downward flow, the average diameter of which is 5–6 km, and the lifetime of the RN varies from 20 to 30 minutes (meaning its radar stage); the RC is displaced at the speed and in the direction of the leading flow.

A **Convective Storm** is a set of radar cells united not only by common external isocontours of reflectivity Z, but also by internal dynamic links that manifest themselves in some spatial and temporal sequence of their emergence, growth and dissipation; feeder cells are an integral part of the storm, the totality of which manifests itself as a flanking line (FL), which is most often not detected by radar; the two parts of the storm - the radar-visible "radar body" and the radar-indistinguishable FL, represent a two-fold unity, constituting an inseparable whole.

Multicell Storm (Multicell)—a convective storm consisting of several interacting quasi-vertical, spatially separated and formed in some sequence of radar cells (RC), which are at different stages of development and shift along the leading flow; the storm, as a whole, deviates from the direction of the leading flow (storm deviation) depending on the magnitude and direction of the evolution vector ($\overrightarrow{V_e}$); the size of a multi-cell storm is up to several tens of kilometres, and its lifetime is up to several hours, as it is constantly renewed by the appearance of new RCs from among the feeder clouds—feeder cells, usually lining up in a line of feeder clouds—a flanking line; an important property that distinguishes storms in general and multicell storms in particular from RCs is the short-term or long-term appear-

ance of a canopy of radio echo covering the area of weak radio echo from above and, partially, from the sides; strong, sometimes catastrophic precipitation, often with large hail up to 2–5 cm and more, as well as strong wind, is associated with severe multicell storms.

Supercell Storm (Supercell-supercel, supercell classical)—a multi-cell storm in which radar cells (RC) are indistinguishable and the arrival of a new cloud resource in the form of feeder cells is quasi-continuous: the presence of a powerful, sometimes up to tens of kilometres in length and width, stationary canopy of radio echoes indicates an equally powerful in size and speed (up to 30–40 m/s or more) upward flow, due to which hail can grow up to 10 or more centimetres in diameter; the most important sign and at the same time distinguishing a supercell storm from a multicell storm is the presence of a mesocyclone (mesoanticyclone), which is localised in the area of weak radio echo (WER) and is often accompanied by the manifestation of hook echo at lower levels, which usually indicates the presence of tornadoes and powerful winds; the size of supercells can reach several tens of kilometres in diameter; lifetime—up to 7–8 and more hours; deviation of a supercell—most often to the right (in the northern hemisphere) —is accompanied by slowing down of its speed from 1.5 to 2.5 times, displacement of a supercell along the trajectory is accompanied by destructive hail storms, powerful winds and precipitation, often with floods, and other dangerous weather phenomena.

Leading Flow (Leading Flow Vector - $\overrightarrow{V_c}$)—wind at 600 hPa: direction (from where) and speed.

The Development, Evolution Vector ($\overrightarrow{V_e}$) is a vector denoting the direction (from where) and the rate of merging of the radar body of the storm with feeder cells. In the LCS, it is determined by the direction and rate of radio echo accretion of a particular convective storm.

The Storm Motion Vector ($\overrightarrow{V_s}$)is the direction and rate of displacement of the convective storm as a whole ($\overrightarrow{V_s} = \overrightarrow{V_c} + \overrightarrow{V_e}$).

Radio Echo Canopy—an elongated part of the radio echo (on vertical sections) of multicell or supercell storms with relatively high Z values, covering from above and partially from the sides the area of weak radio echo, which is a place of localisation of precipitation particles recirculating and growing on the main upward flow.

The Canopy Direction of the convective storm radio echo - horizontal projection of the line connecting the maximum radio echo at the lower level (closer to the ground surface) with that at the level of the maximum horizontal extent of the canopy, usually coincides with the direction of displacement of the convective storm as a whole, i.e. $\overrightarrow{V_s}$; the concept is widely used in Russian research and Russian anti-hail defence technology [3–5].

Storm Deviation (Deviant Storm Behaviour) is a deviation of the storm trajectory from the leading flow, both in velocity and direction, associated with the emergence of new RCs in some part of the storm and simultaneous dissipation of old RCs in the process of storm evolution; depending on the ratio of vectors ($\overrightarrow{V_c}$ and $\overrightarrow{V_e}$) the storm displacement is slowed down or accelerated [2,4,5].

This review paper presents our studies of the last 4 years, in which various convective phenomena have been considered, including those using the LCS technique. When using this technique, the choice of the leading flow is important. There are different approaches to this question. Thus, Hitchfeld [6] chose the wind at a height of 700 hPa (≈ 3 km) as the leading flow. Some researchers, using the <pressure weight> method, integrated the wind at different heights: Newton and Fankhauser [7], 1–12 km (900 hPa to 200 hPa); Fujita and Grandoso [8], and Charba and Sasaki [9], 0–9 km (from surface pressure to 300 hPa); Haglund [10], 0.5–12 km (950 to 200 hPa); Marwitz [11], and Burgess et al [12], 0–10 km (from surface pressure to 270 hPa). Other researchers have also integrated wind at different altitudes using the <density weight> method: Lemon et al [14], Bluestein et al [13], and Kubesh et al [15], 1–12 km (800–200 hPa); Brown [16], 1–11 km (800–330 hPa); Burgess and Curran [17], 1–10 km (800–270 hPa); Conway and Wurman [18], 0–6 km (from surface pressure to

500 hPa). In our studies, we determined the leading flow at a height of 600 hPa, which corresponds to the "centre of gravity" of the part of the troposphere in which convection develops (0–16, 17 km) and also best agrees with the RC displacement.

2. Materials and Method

For the analysis, we used published data of full-scale radar observations of convective storms from foreign and Russian researchers, data from the ACS-MRL5 system (incoherent radar MRL 5 with λ = 10 cm) [3] in the structure of anti-hail protection service (HPS) of the Republic of Moldova and HPS in the regions of the North Caucasus (Russian Federation), as well as various hypotheses and models that consider the dynamics and kinematics of convective storms. These data provided a volumetric picture of the radio echo and multiple parameters with a frequency of about 3.5 minutes throughout the development of the thunderstorm process (THSP). In addition, aerological and synoptic information was used. The radar information was analysed in both the Eulerian Coordinate System (ECS) and the Lagrangian Coordinate System (LCS) and compared where appropriate.

3. Correlation of motion vectors of a convective storm

3.1 General statistical characterisation of kinematic parameters of storms in the North Caucasus and the Republic of Moldova

Figure 1 presents a classical scheme of the development and motion of multi-cell storms depending on the direction of ($\overrightarrow{V_e}$) versus ($\overrightarrow{V_c}$) [19]. New cells in the storm emerge with different frequencies and in a certain direction, the evolution vector ($\overrightarrow{V_e}$). At the same time, each of the RCs passed through three stages: emergence, maximum development, and dissipation, which are separated from each other in time by the value Δt. This scheme shows that storms can move in different ways: either with deceleration (**Figure 1a** and **1b**) or with acceleration (**Figure 1c**), which depends on the orientation and magnitude of the evolution vector. It should be emphasised that numerous studies [4,5,19–30] and especially [31,32] have shown that multicell and supercell storms are not fundamentally different in their dynamics and kinematics. Therefore, the kinematic schemes of the development of convective multicell storms considered below apply equally to supercells.

For our study, 51 cases of the most powerful storms that produced moderate to intense hail and had a well-formed radio echo canopy were selected. Of these, 5 storms were supercells. For some of the long-lived powerful storms that experienced trajectory breaks, the following parameters were also calculated on their rectilinear (quasi-rectilinear) sections. As a result of this approach, the number of measurements used increased to 69 in some cases. The hail intensity gradations in storms were determined by a set of a number of parameters. The main parameters measured are: Zmax-maximum of reflectivity, ΔHZ-excess of the upper boundary of isosurfaces Z = 15 dBZ, 20dBZ, etc. every 5 dBZ above the level of zero isotherm H0°, I-intensity of precipitation, etc. [3].

Note that the maximum reflectivity Zmax over the whole sample varied from 58 to 76 dBZ. The mean value is 65 ± 4 dB. The sample was checked for representativeness by comparing our data with data from 254 storms in Southern Brazil [33]. It showed their high consistency, taking into account the mirror image (northern and southern hemispheres), as well as the similarity of climatic conditions of the regions.

Figure 2c shows that almost half of the storms (49%) were in the hail stage for an average of 30 minutes, another quarter of the total (26%) for about 60 minutes, and 18% of the powerful convective storms were in the hail stage for about 90 minutes. All other most powerful supercell storms accounted for 7% of our sample. The mean lifetime of storms in the hail stage was 55 ± 35 minutes. The mean value of the ratio $\overrightarrow{V_s}/\overrightarrow{V_c}$ across the sample was 0.83, indicating that they were slowing down overall.

The motion of convective storms, as shown above, is in direct dependence on the direction and velocity of their evolution . Numerous radar, e.g., [34,35], aircraft [36–38], and satellite [39,40] studies have found

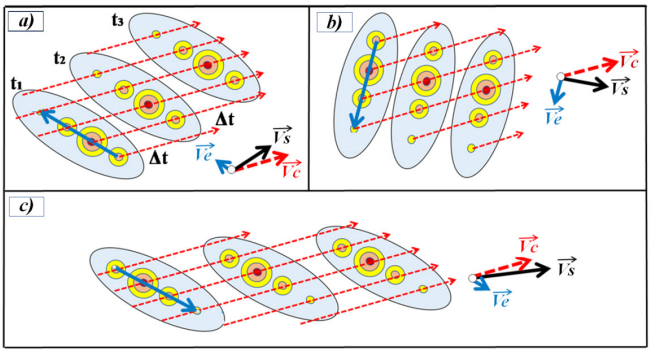

Figure 1. Scheme of development and motion of multicell storms depending on the direction of the evolution vector $\overrightarrow{V_e}$: (**a**) left-back; (**b**) right-back; (**c**) ahead on the right. $\overrightarrow{V_c}$ is the leading flow vector (radar cell displacement vector); $\overrightarrow{V_s}$—the motion vector of the convective storm as a single unit (ECS).

Source: Browning et al.[19]

that this is due to the arrival of a cloud resource in the form of feeder cells (FCs) in the radar body of the storm. It is these FCs that are the object of influence in modern precipitation modification technologies in general and, especially, in Hail Protection Services [3,41,42]. For this reason, the study of this aspect of storm dynamics and kinematics is very relevant.

3.2 Deviations of hail storm canopy directions from their trajectories according to radar data in the Republic of Moldova and the North Caucasus

Figure 2a shows that the distribution of the parameter of the mean canopy orientation deviation from the trajectory is normal with a mode in 48% of the cases falling within the ± 10° gradation; for an individual supercell (**Figure 2b**), the minimum deviation of ± 10° is almost 70%, while the remaining almost 30% of the measurements show a deviation within + 10° + 30°, i.e., to the right of the storm trajectory. These data indicate that the storm-averaged canopy direction is most often the same as the storm trajectory, or at least this deviation is not large. For supercells, these deviations are even smaller, which also testifies to the quasi-stability of their radar echo and, hence, internal flow structure (upward and downward motions).

In the analysis of the THSP of 19 August 2015 in the North Caucasus, which is also the subject of a number of papers by Abshaev et al. [43,44], we found a unique phenomenon that is directly related to the question of the orientation of the radio echo canopy discussed here. It concerns the unusual behaviour of a multicell storm (hereafter it will be denoted as S2-red vector and S2*-violet vector), which existed for more than 2.5 hours. At the same time, for 1 hr. 41 minutes, the storm moved from east to west (during this period it is labelled as S2), towards the supercell, and then in the opposite direction (labelled as S2*) (**Figure 3**).

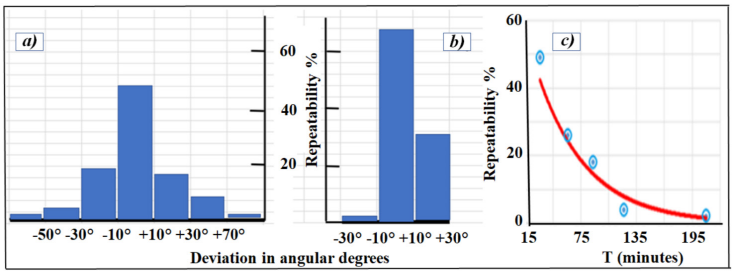

Figure 2. Some summarized data: (**a**) Deviation of storm averages of canopy orientation from the storm direction for the whole sample (69 measurements); (**b**) Deviation of canopy orientation for the supercell (84 measurements) in the North Caucasus from 19.08.2015; (**c**) Recurrence of hail stage duration (in minutes) for the whole sample.

Source:Livshits, et al[2,4,5].

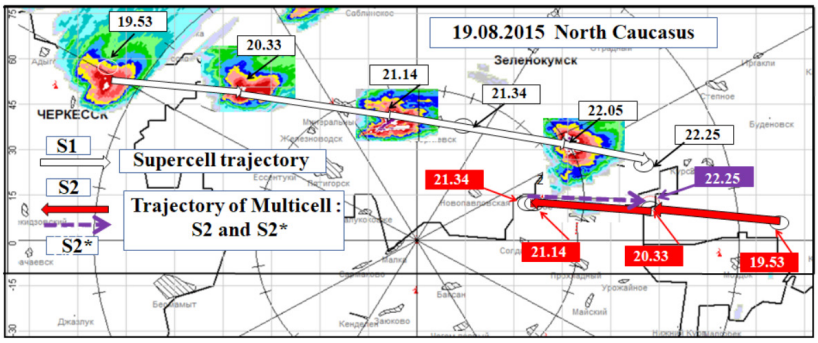

Figure 3. Trajectories: supercells (S1) and multicells (S2 and S2*). 19.08.2015 North Caucasus.

Source: Livshits [2].

The orientation of the supercell canopies (S1) coincided with its trajectory. The orientation of the canopies of the multicell storm (S2 and S2*) also coincided with its trajectory, but in different periods had almost opposite directions, which is well demonstrated in **Figure 4**. The storms moved towards each other: S1—in the eastern direction, and S2—in the western direction. Between 21:14 and 21:34, S2 hardly shifted and its vertical structure showed no canopy (**Figure 4c**). Later, when the storm trajectory of S2 reversed, the orientation of the canopy also reversed (**Figure 4d**).

3.3 Hypothesis on the structure of a cold front of the second kind

The motion of S2–S2* along the trajectory, especially the change of directions and velocities, was a peculiar indicator that allowed us to determine the boundaries and some properties of the cold front of the second kind. We suggested that this unique phenomenon was connected with the presence on this day of a perturbation in the form of the air flow in the direction opposite to a powerful west-east transport. This wind disturbance similar to the leading flow, which controls the motion of convective clouds, could "pick up" S2, drawing it in the direction of the cold front coming from the west.

To explain this phenomenon, we involved calculations using the WRF-ARF prognostic regional non-hydrostatic atmospheric model [45] and data from the European Centre for Medium-Term Weather Forecasts (ECMWF) ERA-5 [46]. The analysis of calculations using these models confirmed the presence of the wind disturbance directly in the area of S2 occurrence. The disturbance from the southeast with a strength of up to 7 m/sec was localised at a height of 700 hPa. Based on the obtained data, it was possible to construct the structure of a cold front of the 2nd kind [2].

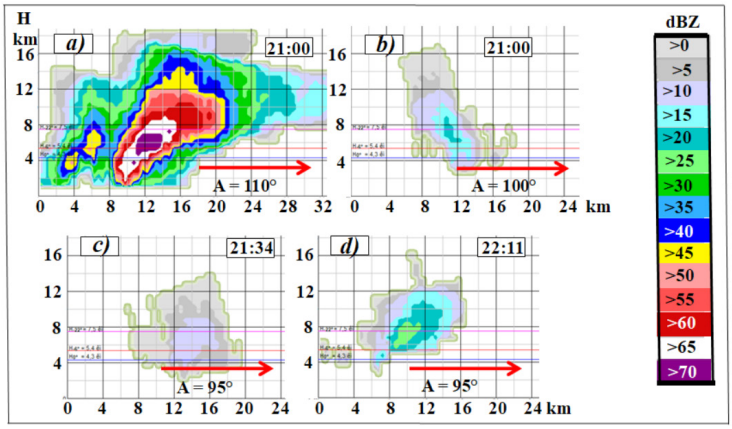

Figure 4. Vertical cross-sections along azimuth: (A-red arrow): supercells—(**a**) and multicells—(**b**), (**c**), (**d**). 19.08.2015 North Caucasus.

Source: Livshits [2].

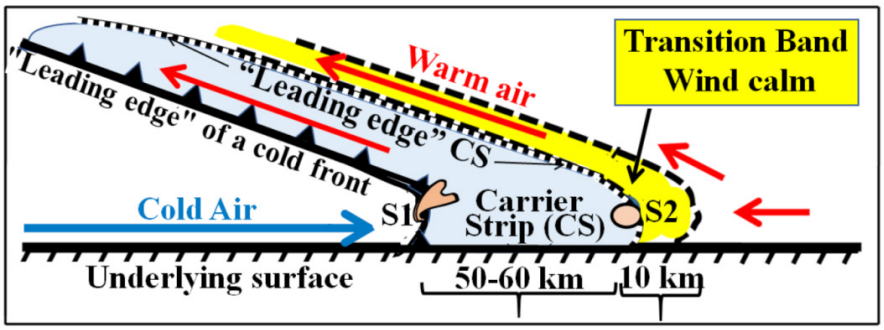

Figure 5. Cross section of the cold front of the second kind 19.08.2015 North Caucasus (Hypothesis).

Source: Livshits [2].

Figure 5 shows the vertical cross section of the cold front of the 2nd type, parallel to its displacement in the general direction from west to east. The cold front of the 2nd type, as we understand it, is first of all a "leading edge"—a certain conventional line separating two air masses: cold and warm air. In warm air, the Leading Edge is followed by a 50–60 km wide "Carrier Strip" ("CS") (shown in grey), and then by a narrow band about 10 km wide ("Transition Band"—shown in yellow). The two bands—the "Carrier Strip" and the "Transition Band"—are separated by a narrow line called the "Leading Edge Carrier Strip". "The Carrier Strip" is an area of warm air that is pushed forward and upward at the Leading Edge Displacement Rate by rapidly moving cold air. This is followed by the "transition band", which is characterised by a "wind calm". Wind calm is not the absence of wind, but a chaotic change in wind direction that does not allow the cloud to "adapt" and "choose" a stable direction of movement [2]. It should be noted that this hypothesis needs additional verification using radar and ground-based observations.

3.4 Repeatability of storm trajectories deviations from the leading flow direction

The distribution of the repeatability of storm trajectory deviations (in degrees) from the leading flow direction (**Figure 6a**) shows that almost one third of powerful storms deviate from the leading flow (29% of all cases) within 10° to 30° to the right, and deviations from 10° to 50° to the right account for 54% of all cases. Similar deviations from 10° to 50°, but to the left, account for 20% and only 12% of all cases deviate within ± 10°.

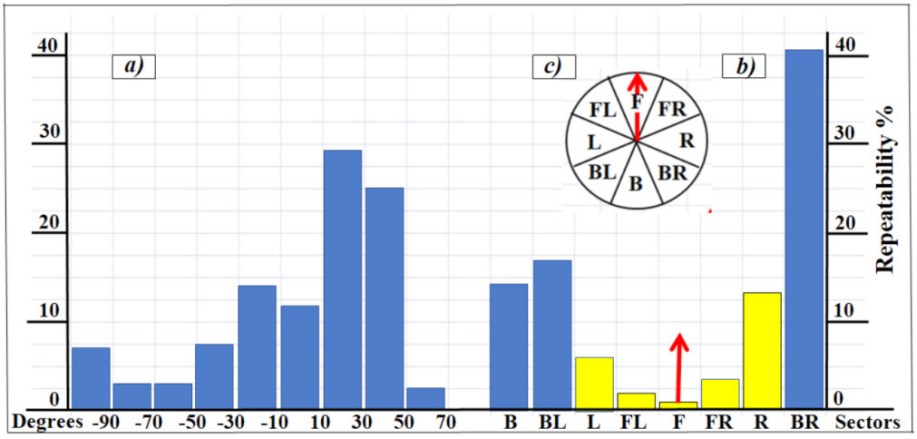

Figure 6. Repeatability of deviations: (**a**) storm trajectories ($\overrightarrow{V_s}$) from the leading flow direction ($\overrightarrow{V_c}$) in degrees by gradations (69 measurements); (**b**) evolution direction ($\overrightarrow{V_e}$) from the leading flow direction ($\overrightarrow{V_c}$); (**c**) scheme of mutual orientation of sectors. The red arrow indicates the direction of the leading flow. Deciphering sector designations: F–Forward; FR–Forward Right; R–Right; BR–Back Right; B–Back; BL–Back Left; L–Left; FL–Forward Left.

3.5 Deviations of evolution vectors from the leading flow direction

Let us consider **Figure 6b**, which shows the repeatability of deviations $\overrightarrow{V_e}$ from $\overrightarrow{V_c}$ by sector. A maximum of 41 % recurrence occurs in sector BR and a second relative maximum of 16 % occurs in sector BL. The sectors in which the storm slows down (blue) account for 71 %, while the remaining sectors (yellow) accelerate. In other words, almost three quarters of all cases are powerful storms developing with a deceleration relative to $\overrightarrow{V_e}$, resulting in a greater or lesser degree of deceleration.

Note also that the number of storms evolving backwards and to the right (BR) is 2.5 times greater than storms evolving backwards and to the left (BL), generally reflecting the tendency for storms to evolve preferentially to the right of $\overrightarrow{V_c}$ in the northern hemisphere.

3.6 Repeatability of deviations of the storm evolution vector ($\overrightarrow{V_e}$) from the mean of the canopy directions (storm displacements—($\overrightarrow{V_s}$)

From the histogram (**Figure 7**), it can be seen that only in sector F (only 9% of cases) there is a coincidence or minimal divergence of the two directions. In all other cases, this divergence increases: the total recurrence of mean deviations ± 45° (sectors FR and FL) is already 25%, the total recurrence of mean deviations ± 90° (sectors R and L) is 40% and the total recurrence of mean deviations ± 135° (sectors BR and BL) is 25%. Important remark: the statistics concerning the deviations of the motion vectors, namely $\overrightarrow{V_e}$ and $\overrightarrow{V_s}$, to the left of $\overrightarrow{V_c}$ refer to left-moving storms; if $\overrightarrow{V_e}$ and $\overrightarrow{V_s}$ deviate to the right of $\overrightarrow{V_c}$, then these statistics are right-moving storms.

Approximately 64% of all storms evolve to the right or left of the canopy at an angle ranging from ± 60° to ± 158°(average ± 109°). Of the total number of storms within these limits, ≈ 48% evolve to the right. These important conclusions will be needed when we correlate the positions of the radio echo from storms and the Flanking Line.

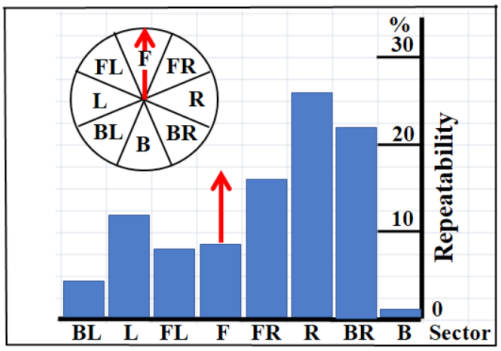

Figure 7. Repeatability of deviations of the evolution directions from the average for the storm canopy directions (storm motion vector) by sectors (69 measurements). The red arrow indicates the direction of sector counting relative to the canopy orientation.

3.7 Orientation of hail bands of convective storms

Hail precipitation, like liquid precipitation, falls directly where the radar cells (RCs) in a convective storm are located. Since RCs consistently arise and evolve in the convective storm system along the evolution vector $\overrightarrow{V_e}$, the orientation of the hail bands should also indicate the direction of evolution. However, it is only in severe hail storms, in which hail precipitation falls simultaneously from several RCs that compose it, that there is a linear elongation of the hail band. This linear elongation should indicate the direction along which the RCs are located in the convective storm. Therefore, it was necessary to find a method of separate fixation of hail bands. Such a method is technically implemented in one of the ACS-MRL subprogrammes in the form of the "Map of hail kinetic energy". A hail band is understood as an instantaneous picture of hail precipitation obtained by a single horizontal scanning at a level close to the ground. Hail Path (Hail Track) means a set of hail bands for the entire period of hail fallout from a convective storm.

Figure 8 shows the general picture of hail paths during the period of supercells passage on 19.08.2015 in the North Caucasus (from 11:37 to 23:58 UTC) through the radius of observation of the Zelenokumsk radar, and **Figure 9** shows a fragment of the hail path from the southern supercell. Its enlarged fragment allows for examining the hail bands in more detail.

The hail bands oriented along the evolution vector (see the ratio of motion vectors in Figure 9) in the southern part are narrow and less intense than the northern ones. This indicates the order in which the storm cells "produce" hail: first—northern, then—southern. Such elongation and narrowing of the hail band in the direction of storm renewal ($\overrightarrow{V_e}$) confirms not only the sequence and order of appearance of new cells in the storm, but also demonstrates that the supercell is a powerful multi-cell convective storm with "weak" evolution [26,27,31].

The orientation and shape of hail bands in severe hail storms help to determine more accurately not only the speed of the storm but also the direction of the Flanking Line. This, in turn, allows for more accurate construction of seeding areas when impacting convective storms.

3.8 Anvil orientation in severe convective storms

The anvil orientation of a severe convective storm is the result of two main factors: powerful horizontal flows at tropopause heights (often jet currents) and a constantly acting moisture source—a powerful upward flow moving along the storm's trajectory (**Figure 10**).

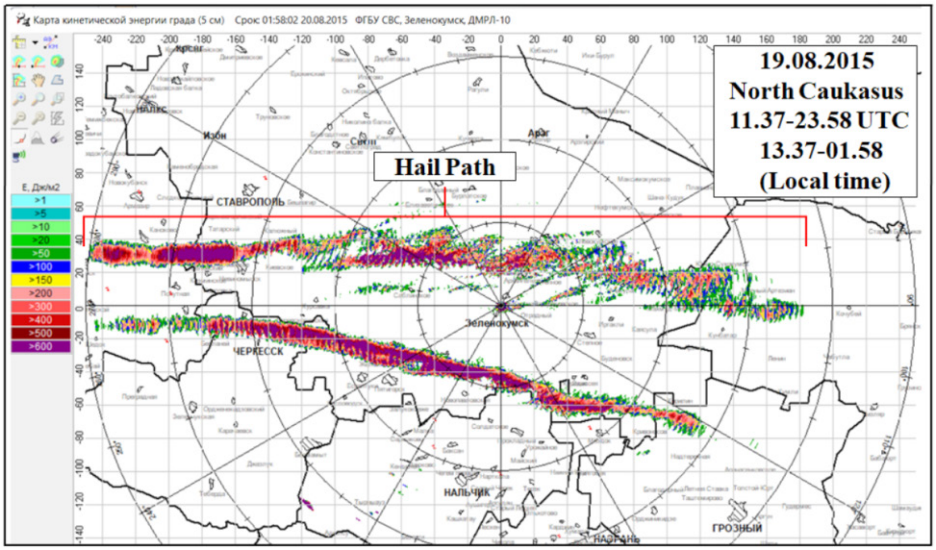

Figure 8. Hail kinetic energy map (Zelenokumsk DMRL-10 radar station. λ = 5 cm). THSP in the North Caucasus from 19.08.2015.

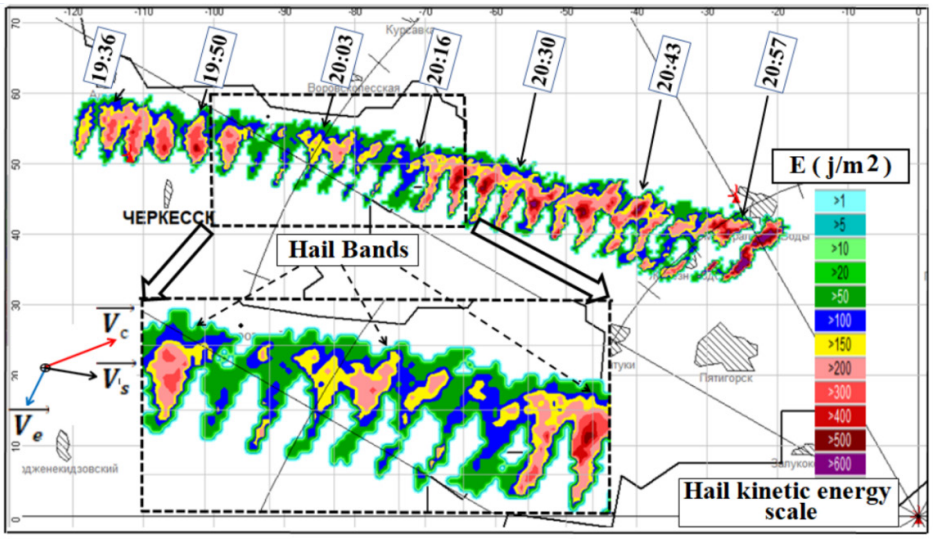

Figure 9. Fragment of the map of hail kinetic energy (map of hail bands and hail track). Black arrows correspond to the time of hail band fixation. Supercell in the North Caucasus from 19.08.2015.

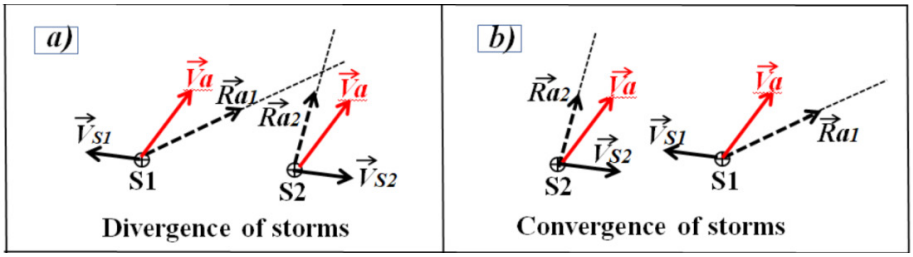

Figure 10. Relationship between the storm motion vectors ($\overrightarrow{V_{S1}}$) and ($\overrightarrow{V_{S2}}$), the external wind at anvil height ($\overrightarrow{V_a}$) and the anvil orientation vectors ($\overrightarrow{R_{a1}}$) and ($\overrightarrow{R_{a2}}$) for storms S1 and S2, respectively, in situations of: (**a**) divergence and (**b**) convergence of storms.

Source: Livshits [2].

We have conducted a study of anvil orientation during storm splitting and merging [2], and reviewed many works, e.g., [47,48]. As a result, two mnemonic rules are proposed.

Rule 1, first:

- if the continuations of the anvil orientation vectors ($\overrightarrow{R_a}$) of two storms intersect—the storms diverge, if they do not intersect—they converge.

Rule 2, more general, applies both to individual storms and to pairs of storms in the process of convergence or divergence:

- if the wind vector at anvil height $\overrightarrow{V_a}$ is to the right of $\overrightarrow{R_a}$—the storm is right-moving;

- if the wind vector at anvil height $\overrightarrow{V_a}$ is to the left of $\overrightarrow{R_a}$—the storm is left-moving.

Applying these simple rules when analysing even a single frame obtained from satellite or radar scanning will allow us to determine the future dynamics of storms: left-or-right-moving storms, divergence or convergence of storms.

A clarification needs to be made. The divergence of storm trajectories may or may not be due to the splitting of a storm into two, or it may not be due to the splitting of a storm: two different storms shift along their trajectories. The convergence of storms does not necessarily mean that they merge.

4. Meso-scale convective structures in the troposphere

Observations from space have shown that Rayleigh-Benard convection is a very common phenomenon in the atmosphere. Fields of such convection simultaneously occupy areas of sometimes several million square kilometres.

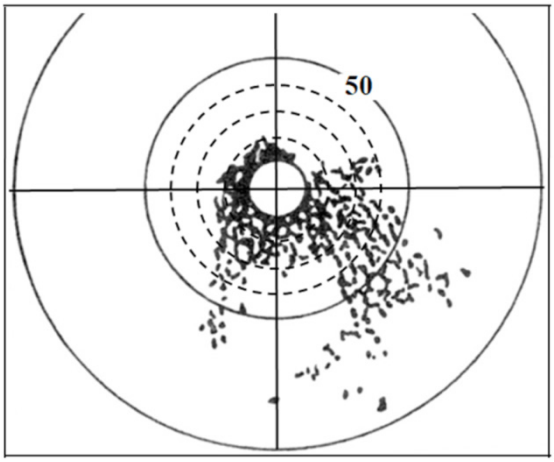

Figure 11. Mesoscale structure of cell convection 20.07.1986. Moldova. MRL-5 (λ = 3.2 cm with the R^2 correction turned off).

Source: Minnachmetov, et al [49].

In Moldova in the mid-1980s [49], radar observations were made and cellular structures in the surface layers of the atmosphere were investigated. **Figure 11** presents the convection pattern obtained with MRL-5 at a wavelength of 3.2 cm with the correction for R^2 switched off, which made it possible to detect cellular convection in a cloudless sky in the surface layer of the atmosphere due to hovering insects. The characteristic sizes of circulating convective cells are 5–10 km, with an existence time of 6–8 hours. Displacement is by flow in the surface layer. Similar results were obtained in a large modern study in Oklahoma [50].

In the pioneering work of 1983 [1], we suggested that cellular convection in the surface layer of the atmosphere is the triggering mechanism for deep convection and that such deep convection should also have a “mesh” polygonal structure (MSCC). In order to test this hypothesis, a Lagrangian approach was used for the first time for this purpose: moving

together with the troposphere (against the leading flow at 600 hPa), the radio echo fields were integrated over a long time interval. Such a technique [1,2] allowed us to detect and confirm the assumption of mesh structures of convective cloud fields at wind shears up to 1 m/sec/km. Analyses of numerous processes with significant wind shears in the troposphere showed that they were dominated by linear structures (MSCL).

By MSCC (Meso Scale Convective Cell) we mean a circulation system with downward motions at its centre and upward motions at its periphery. We refer to the linear elements of the MSCC as facets, which converge at nodes. Under MSCL (Meso Scale Convective Line) we understand quasi-straight-line structures.

We assume that in the process of convection development in the surface layer, due to the translation of mesh convective impulses to the middle and then to the upper layers of the troposphere, the most "lucky" structures with a deviation of linear elements of these structures (facets) within ± 30° from the leading flow "survive". This is expressed in the predominant realisation of linearly oriented structures—MSCL (most often at wind shear >1 m/sec/km).

As an example, we present the analysis of the THSP from 28 June 1982 in the Republic of Moldova (**Figure 12**), carried out in the LCS [51]. The wind shift in the layer from 3 to 10 km did not exceed 1 m/s/km. The THSP is classified, in general, as disordered multicellular processes, according to the classification adopted in Abshaev's study [3]. From the analysis of the integral pattern, it can be seen that radio echoes, developing along linear elements, created clear mesoscale structures in the form of partially or fully formed MSCC and MSCL. Thus, this THSP can most likely be classified as highly organised, and therefore, most amenable to operational forecasting. The Roman numerals from I to IV indicate Meso-Scale Convective Complexes (MSC).

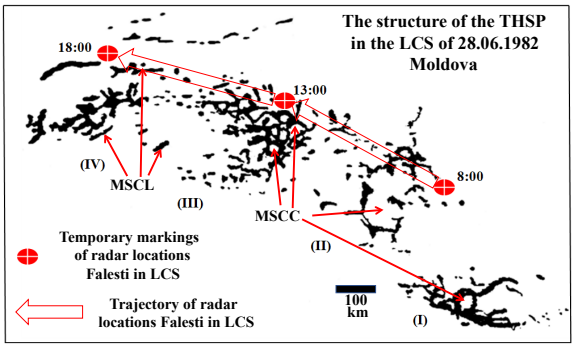

Figure 12. Integral picture of the Thunder and Hailstorm Process (THSP) from 28.06.1982 in the Republic of Moldova (LCS). The time marks of the Faleshti radar station locations are marked by red circles with crosshairs. The movement of the LSC center is shown by a red arrow. The thin red arrows show examples of MSCC and MSCL.

Source: Minnachmetov, et al [51].

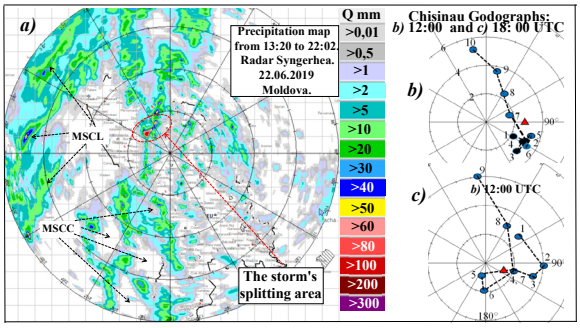

Figure 13. Precipitation field within a radius of 200 km from the radar of Singerei (**a**) THSP from 22.06.2019. Godographs of Chisinau for two terms (**b** and **c**). Black dashed arrows show examples of MSCC and MSCL. The storm separation area is circled with a red oval.

The development of THSP within a homogeneous air mass is demonstrated by the so-called popcorn convection, which is usually characterised as a process without visible convection organisation. An example of this kind took place on 22.06.2019 in Moldova. THSP developed in the region of an eroded low-gradient field of elevated pressure (baric saddle) in the low-moving troposphere. The wind shear across the troposphere was ≈ 0.5 m/s/km. The number of powerful convective storms recorded by 6 radars (radius of radio echo parameters measurement—up to 150 km) was 162; a hail of different intensity was observed in almost 50 storms. **Figure 13** presents a precipitation map for almost 9 hours when convection was noted. Several MSCC and MSCL are shown with arrows. A total of 33 MSCC and more than 10 MSCL were recorded on this day.

Table 1 presents satellite data representing the size distribution of open MSCCs, as well as those obtained from radar observations for 46 TSHPs in Moldova [1]. These data were compared with the results we obtained when analysing the TSHP from 22.06.2019. The maxima of all three distributions occur at MSCCs diameters equal to 30–40 km and are 47%, 37% and 43%, respectively, the other gradations of the distributions coincide or differ slightly. In general, we can state a good agreement of the distributions, and we attribute the small differences to the limited number of MSCCs manifested in a single TSHP.

The THSP under consideration can be classified as highly organised: the clear mesoscale convective formations along which the development of convective storms took place in no way resemble chaos, and the similarity of the three MSCL size distributions obtained from different data may support the hypothesis of mesh convection translation from the surface to the upper troposphere.

At large wind shears in the troposphere, MSCLs predominate, but mesh structures also occur. The development of convective clouds occurs along the facets and at the nodes of MSCC or MSCL. At the same time, the structures do not manifest themselves simultaneously. Convective storms in their development gradually form these structures. It is important that they consist both of radio echoes that actually exist at the present time and of phantoms, i.e., traces of radio echoes that have already collapsed. The construction of such structures in real time is carried out in the LCS with the help of a special subroutine in the ACS-MRL5 system [3].

4.1 Development of convective storms on the elements of the LCS. Kinematics in the LCS

As mentioned above, thanks to the Lagrangian approach, various structures have been found in the time-integrated radio echo field from convective clouds. The development of convective storms is determined by the configuration of the elements of these structures. Obviously, the kinematics of the storms (depends on three factors: the configuration of the elements of the structure, which consists of *facets*—linear elements that converge at *nodes*; on the direction of the leading flow $\overrightarrow{V_c}$ with respect to the facets; on the ratio of the velocities of the leading flow $\overrightarrow{V_c}$ and the evolution vector $\overrightarrow{V_e}$.

With this in mind, let us consider the scheme proposed by Starostin [52], to which we will add some important nuances and new phenomena. These phenomena, discovered by us, will be discussed in the following chapters. The scheme itself will allow us to explain the "behaviour" of storms on MSCC elements.

Table 1. Distribution of MSCC sizes (in %) according to satellite and radar data from work and from TSHP radar data from 22.06.2019 in Moldova.

Data	DiameterMSCC(km)								
	10–20	20–30	30–40	40–50	50–60	60–70	70–80	80–90	90–100
Fromthesatellites	5	21	47	21	3	1	0.8	0.4	0.8
Radar	9	24	37	17	7	3.2	2	0.6	0.2
TSHPdated22.06.2019	6	28	43	17	6				

Source: Livshits [2].

For simplicity, we depict the field of mesoscale convective cells as hexagons with facets and nodes in contact with each other—**Figure 14**. All convective events take place on facets and at nodes. Let us consider them in detail.

In the scheme, nodes are indicated by numbers in circles, and facets by numbers in ellipses.

In nodes:

- two or three facets may converge (nodes 2 and 3)—the *phenomenon of storms merging* and, at the same time, possible *dissipation*;

- two or three facets may diverge (nodes 4 and 1)—*the phenomenon of storms splitting*;

- two facets may enter the node and one facet may leave (node 3)—*the phenomenon of storm merging* and, at the same time, *the phenomenon of trajectory fracture*;

- one facet may enter the node and two facets may exit (node 4)—*the phenomenon of storms splitting* and, at the same time, *the phenomenon of trajectory fracture*;

- one facet can pass through the node and exit also one (node 4)—*the phenomenon of trajectory fracture.*

In addition, the phenomena not described in the study of Starostin [52] and discovered by us for the first time [2,54,55,56] are presented as below.

- *the phenomenon of storm splitting*, in which one of the storms remained in place and continued to develop; this phenomenon is called by us the *"drop splitting phenomenon"* (similar to the picture of separation of a drop of water from a tap, when the drop remaining at the end of the tap spout is again drawn in);

- *double phenomenon—merging of two storms and then their splitting* in the same node;

- a "*nodal" storm* that developed within the node and received updates in an unusual way—directly from the inner regions of the MSCC, rather than from the facets.

Thus, there are 7 possible behaviours of storms in the nodes.

On the facets of the MSCC, storms can:

- diverge (facet 5)—*the phenomenon of splitting*;

- storms can converge (facet 6)—*the phenomenon of merging and dissipation*;

- storms can move parallel to each other—*the phenomenon of pursuit* and, at the same time, *the phenomenon of dissipation* of the storm that has reached the place from which the pursued storm started to move (facet 7, the point marked with a cross).

In total, there are 3 possible variants of storms' behaviour on the facets.

We emphasise that the movement of storms in the LCS is their development, renewal, which takes place along the facets of MSCC and/or MSCL. The exception is the "nodal" storm, which develops due to the resource coming not from the facets, but from the central regions of the MSCC. We will deal with this case in particular.

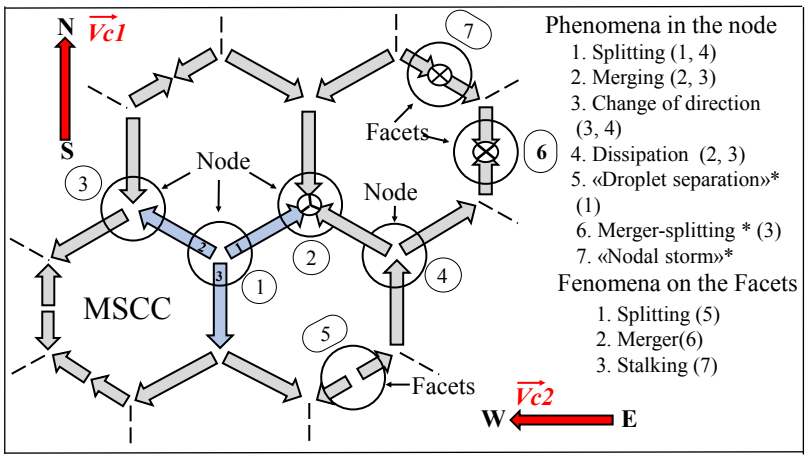

Figure 14. Schematic of the mesh convection structure, on the elements of which storms develop; the phenomena indicated with an asterisk (*) were supplemented. $\overrightarrow{V_{c1}}$ and $\overrightarrow{V_{c2}}$ —leading flow vectors.

Source: Livshits, et al [2,52–55].

Thus, there are 10 variants of storm behaviour on the elements of the MSCC structure, which can be obtained and considered only in LCS.

4.2 Comparison of storm kinematics in LCS and ECS

As an example, let us consider how the trajectories of storms appear to an observer in ECS if the storms evolve from node 1. Let us assume that the storm evolution velocities $\overrightarrow{V_e}$ in all cases are the same and correspond to the magnitudes of the vectors shown in the scale of **Figure 14**.

Consider **Figure 15**, where panels 1 and 2 show different variants of the interaction of vectors with elements of the MSCC structure. Depending on the mutual orientation of the motion vectors, the picture changes significantly. We would like to pay special attention to panel 2, which shows examples of storm splitting at different orientations $\overrightarrow{V_c}$ of relative to the MSCC structure, which explains, among other things, the phenomena of acceleration of a left-moving storm compared to a right-moving storm (b) and vice versa (c), and in **Figure 15a** an example of symmetry of motion of splittings storms. In the further presentation we will express our hypothesis of splitting of storms of different types—supercells and multicells - from unified positions, relying, among other things, on the above examples.

We note that we have not yet varied the absolute rates of storm displacement, nor have we addressed examples for different nodes and facets. If we consider storm trajectories under different variations in ECS, we estimate that the number of variations in the manifestations of the main phenomena could increase to about 120. It follows that the consideration of the kinematics of convective storms in LCS reduces the number of variations by a factor of about 12 compared to ECS. This fact makes the LCS application preferable, as it simplifies and accelerates by more than an order of magnitude all technological methods of radar situation assessment and making prognostic and control decisions in the conditions of constant time deficit (especially when conducting hail protection).

5. Convective phenomena

5.1 Splitting of convective storms

The well-known, which has become classical, the concept [56] suggests that the splitting process consists of two stages: the formation of two rotating (cyclonic and anticyclonic) vertical branches from a horizontally rotating vortex and, further, due to precipitation, the splitting of the supercell into two—cyclonic and anticyclonic. It is believed that the origin of the horizontally rotating vortex is favoured by a specific wind shear with height in the surface layer.

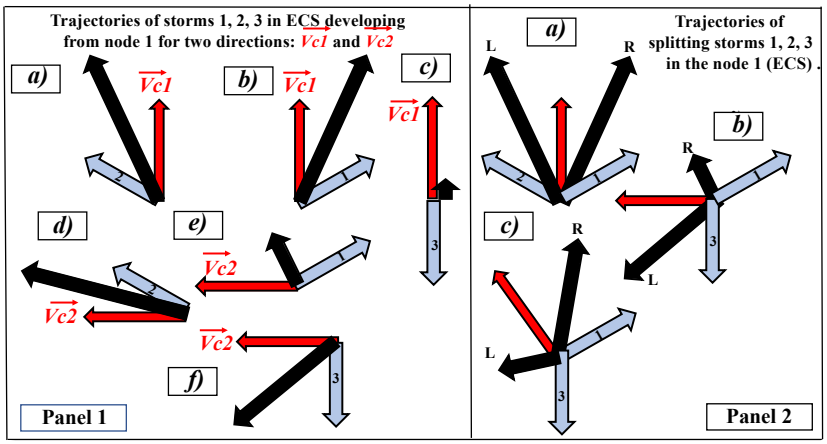

Figure 15. The ratio of the motion vectors of storms 1, 2 and 3 using the example of node 1 from **Figure 14**. Panel 1: (**a**, **b**, **c**) for $\overrightarrow{V_c}$ oriented from south to north; (**d**, **e**, **f**) for $\overrightarrow{V_c}$ oriented from east to west. Panel 2: examples of storm splitting cases with different directions of $\overrightarrow{V_c}$. Notations: red vector— $\overrightarrow{V_c}$; blue— $\overrightarrow{V_e}$; black— $\overrightarrow{V_s}$; L—left-moving storm and R—right-moving storm.

We have carried out a thorough analysis of the literature devoted to this phenomenon in [2, 53,60]. It showed that the splitting of supercell storms in real processes, which are described in detail, for example, by Charba et al [57] and Wang et al [58], do not always agree with theory. In particular, while travelling, the splitting convective storms often changed their deviation from the leading flow from right to left and vice versa. The present study in Bulgaria (Bocheva et al [59]) deals with two cases of supercell splitting on the same day. The first supercell splits into a right long-lived cell (survived 2:35 after separation) and a left short-lived cell (survived ≈ 20 minutes after splitting). In the second case, the supercell split into a left long-lived cell (existed for more than 4 hours) and a right short-lived cell. This case is remarkable because the splitting process occurred differently under the same aero-synoptic conditions: in one case, the right-moving (cyclonic) supercell dominated after the splitting, while in the other case, the left-moving (anticyclonic) supercell dominated after the splitting These and other numerous facts show that the classical concept does not explain such cases in any way.

5.1.1. Splitting of multi-cell storms on the examples of radar observations in Moldova

Figures 16 and 17 show a fragment of the TSHP in Moldova from 19.07.2021, associated with the splitting of the storm, which was assigned the conditional sequence number 36 out of the total number of storms we studied on this day [2,61]. The wind shear with height in the tropospheric layer from 0 to 10 km was 1.4 m/s/km. The leading flow was 250°, 10 m/sec (36 km/hour). S 36 is a multicell hail storm. During development, S 36 split at 21:49 into two—LMS and RMS.

The Zmax value in these storms ranged from 45 to 62 dBZ, and the excess of the top of the radio echo isocontour at 45 dBZ over the 0° isotherm (ΔH45 is one of the parameters determining the hail hazard) was 6–6.5 km. The intensity of falling hail, according to the classification adopted in [3]—moderate. The average speed along the LMS (left-moving storm) trajectory was 29 km/hour and RMS (right-moving storm)—20 km/hour (**Figure 15a**).

The evolution of S 36, represented in **Figure 17** by the radio echo increments—black vectors, shows that LMS evolved with an average speed of 49 km/hour and RMS—21 km/hour. If we assume an average Radar Cell (RC) size of 6 km, the feeder cell fusion rate with the storm for LMS is 8 cells/hour and for RMS is 3.5 cells/hour. LMS lasted 168 minutes and RMS lasted 126 minutes. These facts indicate that LMS dominates relative to RMS in this example.

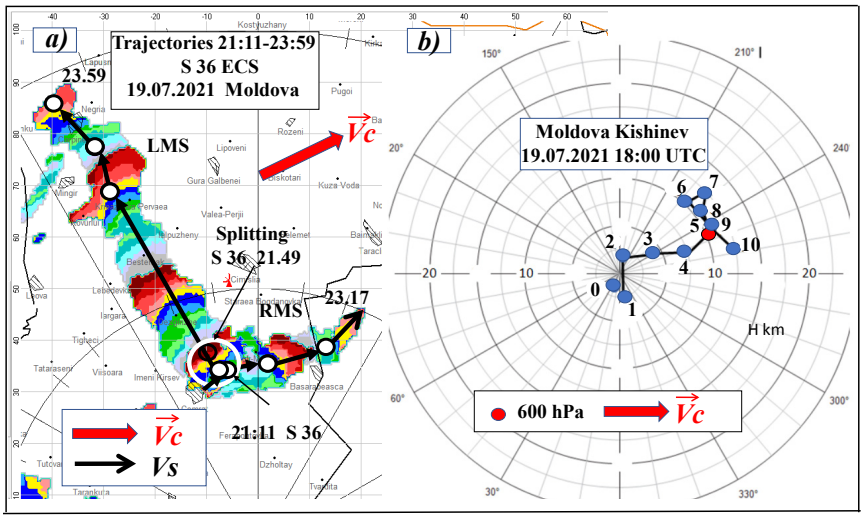

Figure 16. Storm 36 (S 36) splitting at ECS: (**a**) LMS (left-moving storm) and RMS (right-moving storm) trajectories; (**b**) hodograph. Radio echo increment color changes every 3.5 minutes. The LMS and RMS motion pattern corresponds to Z ≥ 45 dBZ at a horizontal section height of 5 km.

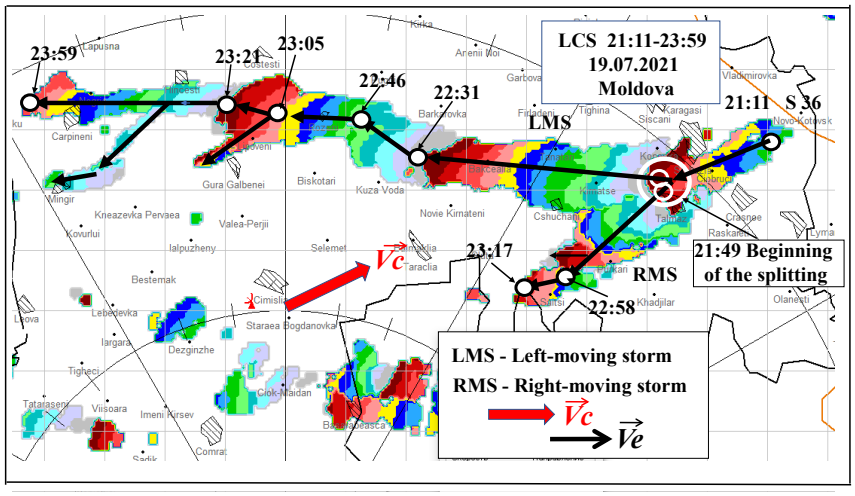

Figure 17. Storm 36 (S 36) splitting at LCS: (**a**) evolution LMS (left-moving storm) and RMS (right-moving storm) trajectories; (**b**) hodograph. Radio echo increment color changes every 3.5 minutes.

5.1.2. The unique separation of the convective storm—"drop separation" 22.06.2019 in Moldova

One of the important fragments of this THSP is related to the behaviour of storm S1, which formed at the MSCC node and existed there for about 1.5 hours. The aerosynoptic context is briefly described in Section 2.

Figure 18n shows a fragment of the integrated structure (LCS) "accumulated" over a period of more than 6.5 hours (from 14:18 to 20:58). In the centre of the figure, the fully closed structure, denoted as MSCS 6, is highlighted in brick colour. The technology of obtaining such structures in the LCS is described in our works [1,2,53,54,60].

To estimate the size of such structures, we assume the diameter of the circle D, equal to the area of the inner region bounded by the lines (we call them "facets"—in Figure 18n these are black lines) drawn through the maxima of all traces ("phantoms") of radio echoes, which eventually formed this closed region of space. The diameter of MSCC 6 is ≈ 14 km. Those parts of this structure, to which special attention should be paid, are highlighted in red.

By the time of S1 formation at 19:01, almost the entire structure of MSCC 6 had already formed: facets 1, 2 4–5 hours before, facet 3–2–3 hours before, facets 4–6 from 1 to 3 hours, and only facets 7 and the northern part of facet 12, represented by storms developing from the south, "docked" to the general structure already in the process of S1 development. Thus, S1, which was formed in the area free of radio echo phantoms of other storms, did not have a special "space" for development. In the future, S2, being detached from the "mother" S1 at 19:42, along the path of its movement formed the facet 10, and further at 20:06, S3 detached from S2, which along the path of its movement formed the facet 11.

The uniqueness of the S1 splitting is that after S2 was separated from it, it remained in place for about 45 more minutes before complete dissipation. Moreover, it intensified for another 25 minutes (**Figure 19c**). The splitting process was studied in detail [2,60] and outwardly resembled the process of separation of a drop from a tap, when the drop remaining on the spout of the tap is pulled inwards (hence the name of this phenomenon—"droplet separation"). Calculations of the growth rate of hail centre volumes at the growth sites of the parameter ΔH55dBZ (indicated by asterisks in **Figure 19c and 19d**), showed that in node 1 this rate is 3 times higher than at node 10 [2]. The fact that S1 remained in place at the MSCC node for 1.5 hours, and evolved more intensely than the S2 that separated from it (**Figure 19d**), makes this situation unusual. In all the cases of storm splitting we observed, the storms left the nodes without delay, continuing on their trajectories following the directions of the convergence zones. In places where nodes are localised, these convergence zones diverge and the directions of resource input to the storms also diverge.

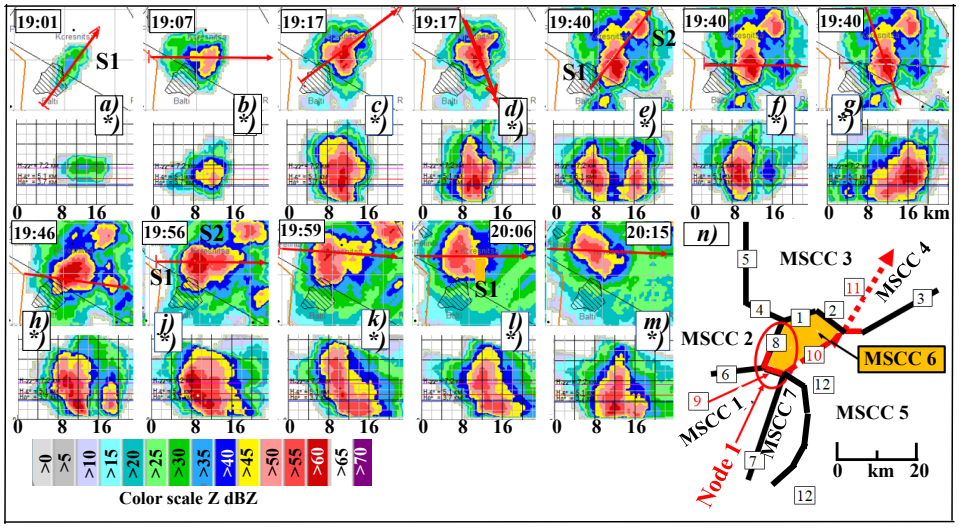

Figure 18. 22.06.2019. Moldova. S1 splitting process: (**a**)–(**m**)—horizontal cross sections at 5 km altitude (red arrows indicate the directions of vertical cross sections); (**a***)–(**m***)—vertical cross sections; (**n**) fragment of the THSP integral structure (in LCS).

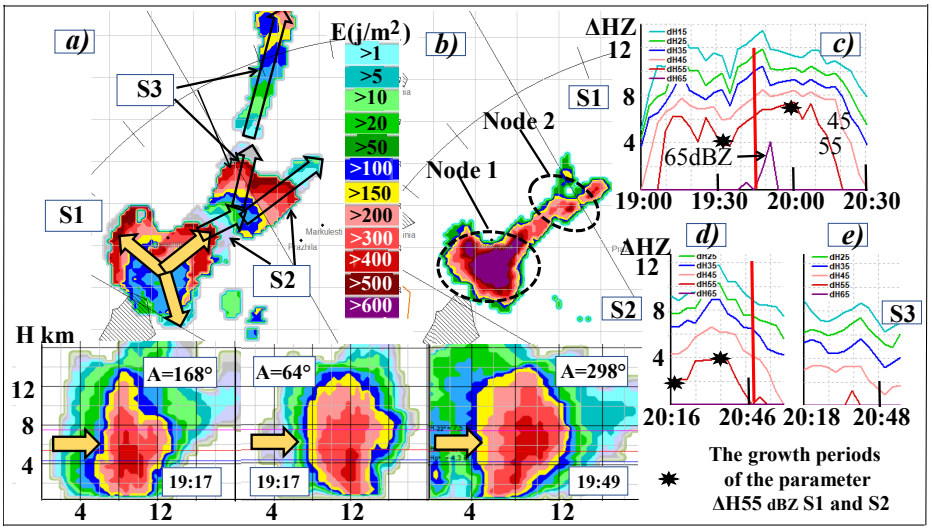

Figure 19. THSP from 22.06.2019. Moldova: (**a**) Storm trajectories (S1,S2,S3). Splitting of storms S1 and S2; (**b**) hail track—kinetic energy of hail (j/m2); (**c,d,e**) course of radar parameters (*Δ*HZ) of storms. Dotted ovals are the localization of MSCC nodes. Brick-colored vectors on the horizontal and vertical sections indicate the directions of the three S1 canopies. The vertical red line in **Figure 19c, 19d** denotes the splitting moment S1 and S2, respectively. The growth periods of the parameter ΔH_{55dBZ}, which also describes the growth of the hail center volume (Q—not shown on the graph), are indicated by asterisks.

We have shown [53,60] that the mechanism for the splitting of multicell and supercell storms is their renewal on different flanks of convective storms and this renewal is associated with the resource input from MSCC facets that diverge from the nodes. It is noteworthy that the development of S1, which in this case is associated with the directions of the radio echo canopies, did not come from the facets but from the inner regions of the MSCC. Moreover, this storm update at some moments, e.g. at 19:17 occurred simultaneously from the side of two different MSCCs (see the vertical cross sections in **Figure 19** and combine them with the overall structure in **Figure 18n**). At other moments, e.g. at 19:49, the directions of the canopies reversed their orientation.

We are particularly interested in this situation in how S1, while remaining in the node for 1.5 hours, received additional impulses for its development without shifting along the facets of MSCC 6, but we will discuss this in a later chapter 5.1.2.

5.2 Merging of convective storms

Convective storm mergers are the most common of all the phenomena associated with Cu cong and Cb, and a large number of papers have been devoted to studying them. They describe various mechanisms leading to cloud merging. Let us recall only some of them: convergence at low levels [27], *interaction of wind shear and downward flows* [27,64]; *pressure gradient between two storms at different stages of development* [65,66]; *upper-level outflows* [64], *different propagation velocities of two storms* [27,67], *increase in the horizontal dimensions of converging clouds* [64], and *cloud rotation* [68]. With the process of mergers of convective clouds, many researchers associate the appearance of a *"cloud bridge"* that unites two radio echoes from the middle level with propagation to the ground [27,64,65]; *increased lightning (thunderstorm) activity* [69–71], *increased volumes of merging clouds, increased radar reflectivity Z, cloud height, intensity and total amount of precipitation, precipitation areas* [72–76], and so on. The *efficiency* of the merging process, according to the authors of numerical experiments with a three-dimensional model, *depends on the thickness of the surface layer* [66] and/or *on the mutual location* of merging clouds *and wind shear* in the troposphere [77].

We found that many studies, e.g., [27,64,72–74,76], did not distinguish between cases of Cb mergers with their feeder cells (Cu cong) and cases of mergers of storms proper. It is important to distinguish between cases of feeder cell mergers with the storm and storm mergers, because feeder cell mergers with the storm are a natural evolutionary process of any convective storm and the only way for it to exist. At the same time, there is always a strengthening of the storm (at the stage of its development) or a slowing down of the decline of its parameters (at its general weakening). The destruction of the storm is connected precisely with the fact that the formation of feeder cells in the storm system stops due to the lack of convective resources. Therefore, too, conclusions about merger outcomes without accounting for differences between individual groups do not objectively reflect the physical processes of mergers. In order to separate the statistics, a special algorithm was developed that allowed us to recruit 138 cases of mergers of only hail storms in the Moldavian region [2,54].

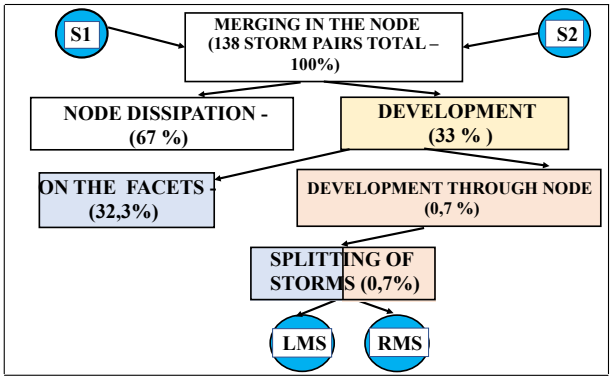

Figure 20. Relationship of different types of merger effects of severe multi-cell hail storms. LMS and RMS—left-moving and right-moving after splitting storms. S1 and S2 are a pair of merging storms.

Our data, plotted in **Figure 20**, show that 2/3 of all merger cases lead to dissipation of merged storms in MSCC nodes. 33% of the storms continue to develop after merging: 32.3% along the MSCC facets, one case of development in a node (0.7%) is associated with the so-called "double phenomenon" (first merging of two storms in a node and then, after some time, splitting), which will be discussed in another chapter. The results obtained do not coincide with those of other researchers, e.g. [27,64,74], who claim that storms almost always intensify as a result of mergers. We attribute this discrepancy mainly to the fact that these researchers did not set themselves the task of distinguishing between two fundamentally different merger processes: feeder cells with their "parent" Cb and storms among themselves. We also attribute certain statistical nuances to regional peculiarities.

The following are examples of hail storm mergers. The first of them is the TSHP fragment of 19.07.2021, which belongs to the most widespread group of mergers with subsequent dissipation of the merged storm in the node.

5.2.1. Storm merging followed by dissipation at the MSCC node

This TSHP developed under the influence of a cold occlusion front at the background of the pe-

riphery of the anticyclonic ridge. The wind shear in the layer from the ground to 8 km was about 2 m/s/km, the wind direction in the same layer was almost unchanged—from the SW, and the leading flow (600 hPa) had a speed of 25 km/h with A = 254°. The height of $H_{0°}$ = 4.25 km, $H_{-6°}$ = 5.2 km, and $H_{-22°}$ = 7.5 km. **Figure 21a** shows the kinematics of storms 5 and 6 (in the LCS), which were 45 km apart at the time of 14:33. In the process of development, these storms were getting closer and at 15:38 a "touching" was observed, and then, at 15:41, a "merger" proper. By "touching" we understand the situation when the Z = 45 dBZ isocontours of the two storms touch for the first time, and by "merging" we understand the situation in which the previous radar image of the storms (at Z ≥ 45 dBZ) is lost and a new, common radar image appears. In this case, all features of the multicell storm are preserved: local maxima and peaks are visible and can be tracked in time.

The vertical cross sections, which are drawn in the direction of the storm trajectories, show that the storm canopies are oriented along the directions of the trajectories [4,5]. The plots of the course of the ΔHZ parameters (**Figure 21n**, **p**) show that the maximum development of S5 and S6 occurs at the moments preceding the merger. Further, there is a sharp decline in parameters and dissipation.

The dynamics of the merging process and its termination with further dissipation took place at the node of the MSCC, where the linear elements—facets—converged. Such merging of storms ends with their complete destruction, as there are no conditions for their development—they have nowhere to develop. It should be noted that this refers only to the most widespread group of mergers—the merger of storms with subsequent dissipation (67% of cases), in another group of storms—(33% of cases) their development after the merger continues.

5.2.2. Storm merger with subsequent development along the MSCC facet

One of such examples refers to the TSHP of 23.07.2014, which developed under the influence of the occlusion front passing over southern Moldova in the background of the Black Sea cyclone. The winds in the troposphere were weak from 4 to 8 m/sec SE and S rhumbes. The wind shear with height was less than 1 m/sec/km. Leading flow with Ac = 180º, Vc = 24 km/hour. $H_{0°}$ = 3.6 km, $H_{-6°}$ = 4.5 km, $H_{-22°}$ = 7.0 km. The distance between S70 and S71 (70 and 71 are notional storm numbers) at the time of the latter's occurrence at 15:24 was 14 km. S70 developed in the W-SW direction, and S71—in the WSW

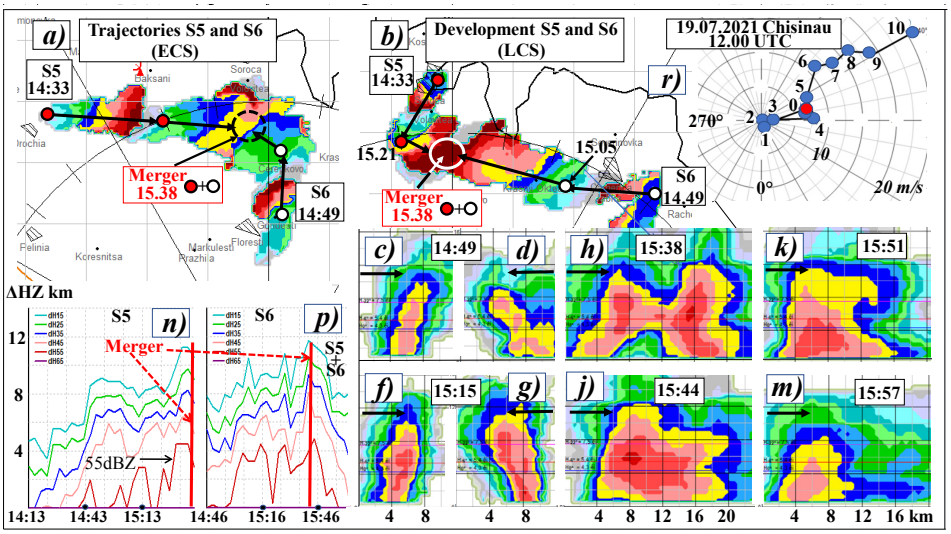

Figure 21. TSHP of 19.07.2021. Moldova. Merger process of S5 and S6: (**a**) trajectories of S5 and S6 at 5 km altitude (corresponding to 45dBZ isocontours); (**b**) integral pattern at 5 km altitude (corresponding to 45dBZ isocontours) in LCS; (**c**–**m**) vertical cross sections through S5 and S6 in the direction of the trajectories; (**n**, **p**) course of *Δ*HZ parameters; (**r**) hodograph; black vectors on vertical cross sections correspond to S5 and S6 trajectories.

direction (in the LCS), the convergence angle was ≈ 150°. By the convergence angle, we mean the angle between the evolution vectors of the approaching storms (in the LCS), which is always smaller than 180° (**Figure 22b** with insets f and f*). Both storms had hail parameters by the time they touched and then merged at 16:55 and continued to evolve after the merger. The merger started from the middle levels and propagated upward and downward, and after the merger, the combined storm changed its direction and continued to develop in the S-SW direction along the MSCC facet until complete dissipation at 17:28, which is confirmed by the course of ΔHZ parameters (**Figure 22c**).

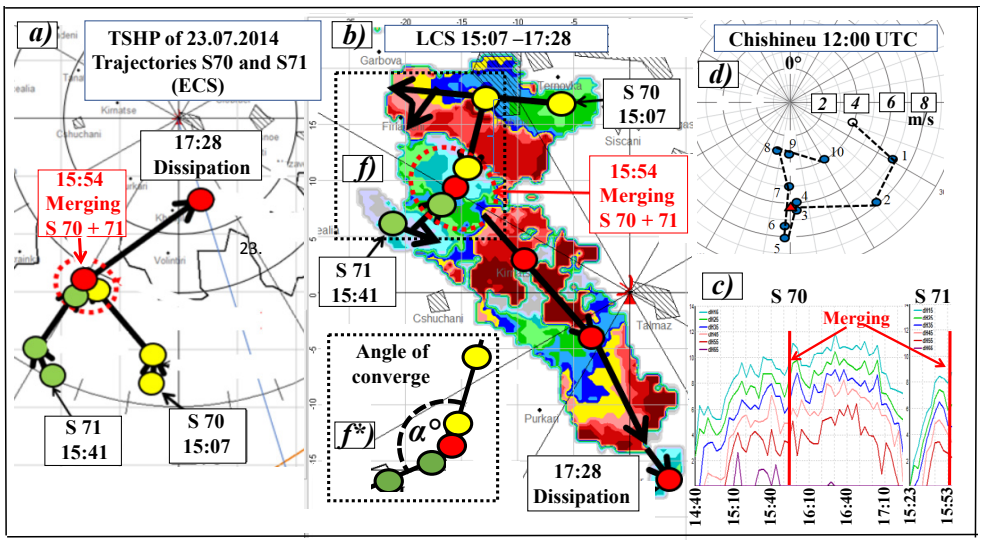

Figure 22. TSHP from 23.07.2014 in Moldova. Merger of storms S70 and S71: (**a**) trajectories; (**b**) integral structure of the merger process and subsequent development of S70; (**c**) course of *Δ*HZ parameters; (**d**) hodograph, red dot—leading flow at 600 hPa; f and f*) insets in (**b**) showing the angle of converge the two storms.

When storms converge, it is found that storms that formed at large distances from each other: from 9 to 45 km (e.g., TSHP from 19.07.2021) merge. It is unlikely that in these cases one can envision merger mechanisms involving short-range interactions. We can assume that such mechanisms operate in the storm-feeder cell system. When it comes to the interaction of storms distant from each other at much larger distances than the average diameter of the radar cell, i.e., more than 5km to 6 km, this mechanism, in our opinion, is meso-β-scale convergence, which stimulates upward motions on scales larger than the storm scale. Such convergence is realized in the form of polygonal mesoscale structures—MSCC and/or mesoscale linear structures—MSCL [54,55].

5.2.3. Hypothesis on the mechanism of merging of convective storms

From our analysis of 138 cases of storm mergers, two of which were considered in the previous chapter, it becomes obvious that the merger phenomenon is also associated with the development of storms along the facets and at the nodes of the MSCC. This development occurs due to feeder clouds, which are lined up in the form of Flanking Lines whose orientation also coincides with the direction of the MSCC facets. With this in mind, we hypothesise a mechanism for the merging of convective storms, which is shown in **Figure 23**.

The merging process of two storms is represented as the intersection, overlapping over each other of the feeder cloud lines of the two approaching storms. It is important to recall that the Flanking Line means a line on which convection in the form of Cu cong already exists. This means that updrafts already exist in each of the feeder cells and the process of cloud particle aggregation has started. When Flanking Lines overlap each other, one can expect the strengthening of convection, as well as the acceleration of manifestation as a result of merging,

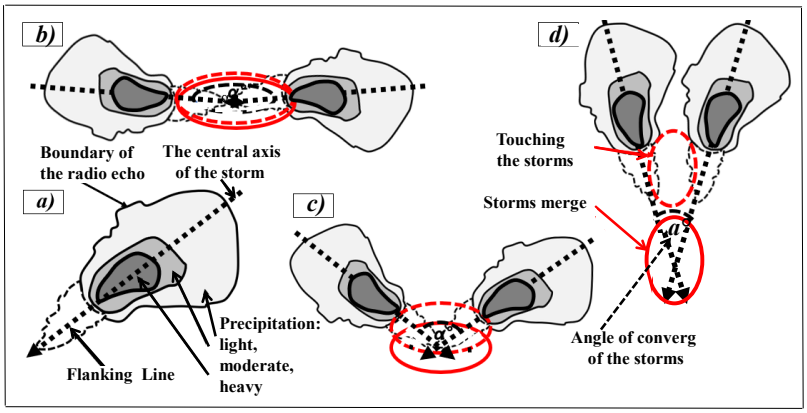

Figure 23. Storm merger hypothesis: (**a**) convective storm scheme; (**b**)–(**d**) storm merger patterns as a function the angle of converge value α°.

previously invisible, and now intensified, becoming radio echoes, feeder cells. At the same time, angle of converge α° formed by the converging "central axes" of storms (dashed lines) can be different: **Figure 23b** and **23d** show their limiting values, and **Figure 23c** shows an intermediate value. Depending on this, the processes of "touching" and "merging" are separated from each other both in space and time: at large angles α° the place and time of "touching" and "merging" are usually close, while at small angles they are distant. Sometimes, at small α°, the storms approach each other only by "touching".

Sometimes, at 45° < α° < 180°, one can observe how, as a result of the interaction of two flanking lines, a "free-standing" radio echo appears between the approaching storms (this case is not presented in the examples we have considered), which is not in contact with any other even at the level of the smallest Z values. In the future, this can be a kind of "bridge" for the simultaneous merging of the three storms. It can be seen that at large α°, the proximity of the flanking lines to each other means a faster "manifestation" of their conjugation sites along the entire length of the flanking lines. This is often observed as an almost simultaneous manifestation of a rather extended, linearly stretched common radio echo. Such phenomena can be detected during the formation of squall lines. However, this is a topic for a separate study.

5.3 "New" convective phenomena

In this chapter, we will present several "new" convective phenomena not previously reported in the literature. Perhaps, these convective phenomena have not been described precisely because the observations were carried out exclusively in the Eulerian coordinate system, which does not allow us in many cases to "see" the nuances of the development of convective storms. Earlier we showed that considering the kinematics of convective storms in the LCS reduces the number of variations by a factor of about 12 compared to the ECS. We believe that this allowed us to discover some "new" convective phenomena, and to look at some well-known ones, e.g., single-cell "storms" from a different point of view.

5.3.1. Double phenomenon: "merger-splitting"

Figure 24 presents a fragment of the TSHP from 05.08.2014, which developed under the influence of the occlusion front at the background of the front of the Black Sea depression. The winds by heights were weak, not exceeding 5.5 m/s up to a height of 10 km, of variable directions. The leading flow: Ac = 319°, Vc = 9 km/h, wind shear—less than 1 m/s/km. At 12:42, when both storms were recorded simultaneously, the distance between them was 16 km. The integral patterns of **Figure 24b** show the trajectories of S61 and S62 (ECS), while Fig. 24a shows the development of the mentioned storms in the LCS. The horizontal and vertical cross sections (**Figure 24d–**

f*) show how these storms gradually converged. As a result, a touchdown was observed at 13:10, and by 13:17 the storms merged, while the individual properties (isocontour Z tops, Zmax positions) were not completely lost. The merged S61 + 62 slightly strengthened (not shown in **Figure 24**) and, what should be emphasised, it, being in the MSCC node, stopped shifting (in the LSCC), i.e. its evolution rate $\overrightarrow{V_e} \approx 0$. The storm remained in the same location in Lagrangian space until 13:31, when the separation of the storms was noted and subsequently they began to shift along different trajectories with evolution velocities $\overrightarrow{V_e}$ up to 25–29 km/hour.

Let us emphasize the fact that the merged storms intensified exactly in the node, receiving resources not from the facets, but in some other way. This will be discussed in Chapter 5.3.2, where another phenomenon—the "nodal" storm—will be presented and a hypothesis explaining this unique phenomenon will be stated.

5.3.2. A "nodal" convective storm. Hypothesis about the mechanism of its functioning

We understand the development of convective storms as an inflow of cloud resource in the form of feeder cells, the linear set of aggregate (Flanking Line) is built along the facets of meso-β-scale structures (MSCC or NSCL) [53,54,60,61]. Such a development is traced in the Lagrangian coordinate system as a linear increment of the radio echo, i.e., as motion. For this reason, the absence of motion and, hence, development in the LCS, while the parameters of the convective storm under consideration indicate its intensification, requires a search for mechanisms that could resolve this obvious contradiction.

In references [2,55], it was shown that the orientation of storm radio echo canopies and hail bands for slow-moving processes coincides with the directions of the facets of meso-β-scale structures. It is from these directions that storms receive feeding in the form of feeder clouds. In Chapter 5.1.2, we considered the unusual behaviour of storm S1 (**Figures 18** and **19**), which for 1.5 hours, remaining in place, received convective impulses not from the MSCC facets (the convective resource on them was exhausted), but in a different way. Based on the results of these studies, let us also consider **Figure 25**, where hail bands and their orientation (as vectors of different colours) are presented.

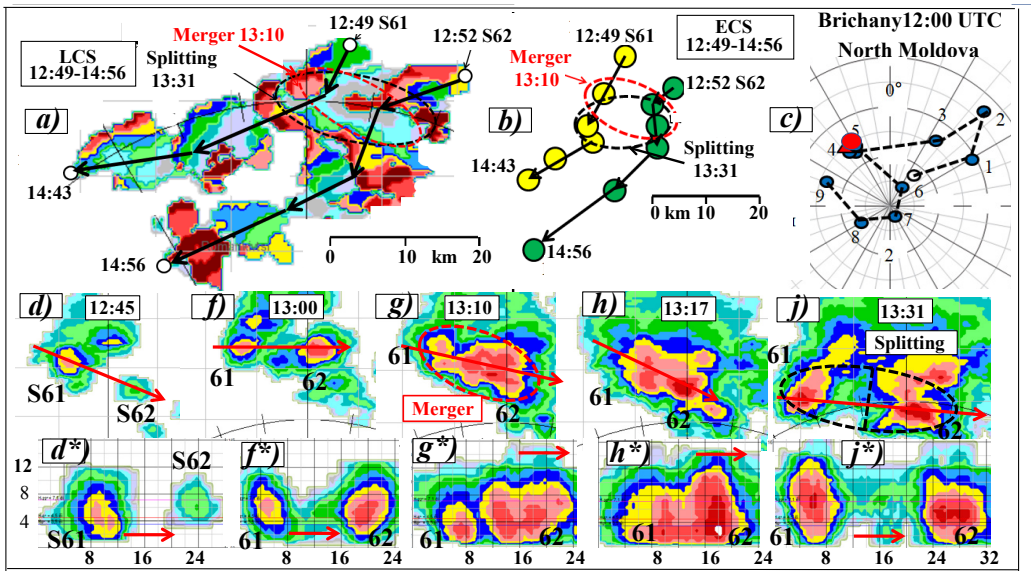

Figure 24. TSHP from 06.08.2014 Moldova. Double phenomenon: "merger-splitting". Horizontal sections at 4.6 km altitude (T° = –6°): (**a**) integral picture in LCS; (**b**) S61 and S62 trajectories in ECS; (***c***) Brichany (North of Moldova) 12:00 UTC hodograph; (**d, f, g, h, j**) horizontal sections; (**d*, f*, g*, h*, j***) vertical sections.

Source: Livshits, et al [54].

The first small hail centre was observed at 19:11 (in the form of a circle with yellow filling). Further, at 19:27 and 19:43 the orientation of hail bands is directed towards the centres of MSCC 6 and MSCC 7. At 19:57, the orientation is towards the centres of MSCC 6 and MSCC 1; at 20:15, the orientation at MSCC 6 and MSCC 1 is retained but a direction towards MSCC 2 is added. The hail process at the node ends by 20:28 and appears as a small patch orientated towards MSCC 2. Most often the resource comes from different directions simultaneously (see in particular the directions of the canopies on the vertical sections of S1 of **Figure 19**). It should be emphasised that the file-by-file analysis (every 3.5 min) showed that the change of directions of resource arrival in S1 did not occur in a continuous manner (as a result of the gradual reversal of the hail band), but in a discrete manner. This means that as the convective resource in one part of the meso-β-scale structure ran out, it began to arrive from another direction or from several directions simultaneously.

Let us turn to **Figure 26**, where we consider in more detail the factors and possible mechanisms of interaction between two convective objects: the MSCC and severe convective storm that arose and developed in the node for 1.5 hours.

In fragment (a), the convective storm (Cb) is labelled at the node, from which precipitation falls. Due to this, a cold pool (shown as a black dashed circle) is formed and spreads in all directions. The leading edge of the cold pool is essentially a gust front. Let us also assume that the MSCC edges have already been "realised" by storms that developed earlier, and that this area along these facets was occupied by cold pools: Let us call them conventionally "old cold pools" (in fragments b) and (c)—these are grey lenses).

Now let us consider two situations in more detail. The first is when the gust front propagates towards the flows from the centre of the MSCC (fragment b), direction Cb—(B). In this case, the two flows from the collapsing part of Cb and from the MSCC meet, which favours the initiation of upward convective motions and the appearance of feeder cells in the form of an arc along the gust front. The second is when the gust front propagates along the MSSS facet, and there is no counterflow on this path, so convection does not occur. As the feeder cells develop, they enter the radar body of the storm and the radio echo canopy(s) on one or the other side of the storm is observed. As for the Flanking Line, its location in a kind of semicircle on the gust front makes this situation unusual. As a rule, the Flanking Line is lined up on the gust front in the form of a "ladder" with a length of 20–30 km, but in this case it forms a semicircle adjacent directly to the storm.

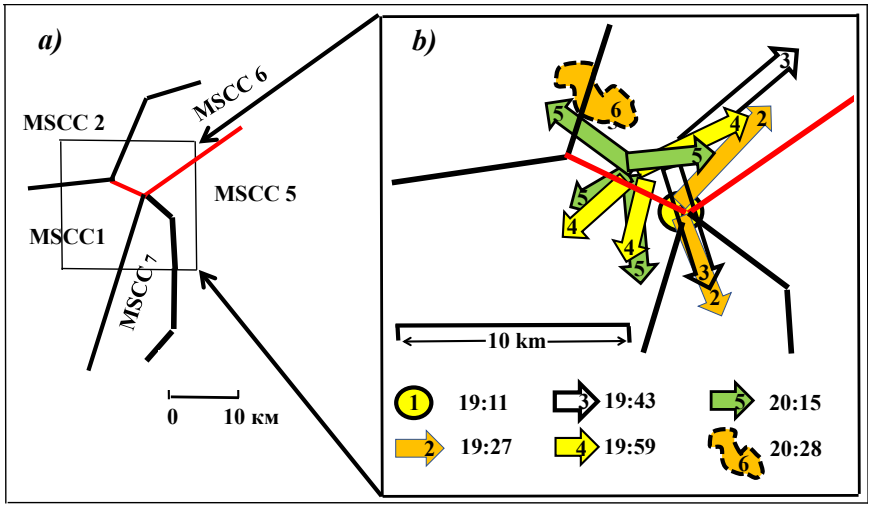

Figure 25. TSHP from 22.06.2019 in Moldova. Changes in the orientation of S1 (**Figures 18** and **19**) hail bands at different moments of time: (**a**) fragment of the meso-*β*-scale structure (LCS); (**b**) orientation of S1 hail bands as vectors of different colour.

Source: Livshits [2].

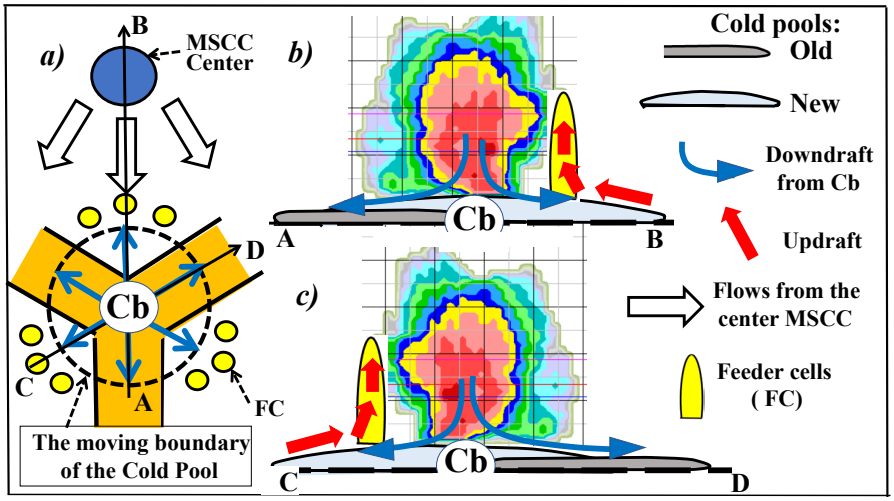

Figure 26. "Nodal" convective storm: (**a**) fragment of the MSCC horizontal cross-section, (**b**) vertical cross-section of the "nodal" storm along line A—B; (**c**) vertical cross-section of the "nodal" storm along line C–D.

Source: Livshits, et al [2, 55].

This type of Flanking Line, as it can be assumed, took place in this particular case. A possible confirmation of this is the research of Bluestein [78], who found 3 types of Flanking Lines, one of which he called a "Vertical Flanking Line". Such an Flanking Line adjoins directly to the storm in the form of an arc, as shown in **Figure 26**.

The described "ideal" mechanism of interaction of different flows (from storm and to storm) depending on the configuration of MSCC elements (facets and nodes) is also superimposed on the dynamics of formation of cold pool fields on the real underlying surface. Indeed, here we deal with the superposition of the processes occurring in the moving troposphere (Lagrangian coordinate system) and the trace in the form of precipitation and cold pools left by moving convective storms on the earth's surface (Eulerian coordinate system). It is the interaction of these processes in the two spaces that can make adjustments to the "ideal" scheme: in one case to promote the occurrence of convective storms of any type, including "nodal" storms, in the other—to prevent it.

5.4 Single-cell convective "storms"—Myth or reality?

In reference [2], we described the results of observations of the initial moments of convection development on the MRL 5 radar with a wavelength of 3.2 cm with R^2 correction switched off within a radius of up to 10 km. This gave a "gain" in radar sensitivity of ≥ 20 dBZ, which allowed us to detect objects inside the Cu cong at the moments of their transition to the initial Cb stage. Objects called "nuclei" were detected, 400–1000 m across, tightly adjoining each other. The diameter of such clusters of nuclei was 4–5 km. On a vertical section they looked like symmetrical objects from the condensation level to a height of several kilometres. At switching on the device of multicontour radio echo display all this picture disappeared and was outlined by only one contour (≈ –20 dBZ). When convection intensified, the picture described above quickly disappeared and the "thin" structure was no longer distinguished. Thus, it turned out that the radar objects that looked like single-cell objects were not actually such, but consisted of many smaller objects—"nuclei". It was concluded that the "single-cell" clouds were in fact multicell clouds, but for technical reasons their multicellularity was not obvious.

In reference [79], the authors studied a large number of "single-cell" storms in the North Caucasus. One of the important observations they noted, as did the Abshaev et al [3], is that "single-cell" storms in processes with weak winds (up to 25 km/hour) moved in any direction at different speeds, i.e. their "chaotic behaviour" was observed. The reason for

this they consider the influence of rough terrain. At the same time, when these objects moved from mountainous areas to plains, where the influence of altitude difference and slope orientation can be neglected, they "behaved" also "unpredictably".

Let us consider one of the TSHP episodes of 22.06.2019 in Moldavia, which could be categorised as a process with "single-cell" convective storms. The aerosynoptic context of this TSHP is described in Section 3, so we will go straight to the description of the part of the process we are interested in. We turn to **Figure 27**, which shows a fragment of the precipitation distribution map for the entire TSHP. Since the leading flow (Ac = 113°, Vc = 10 km/hour) is weak, and the time of existence of the considered storms is significantly less than an hour, the integration of precipitation does not significantly "blur" the final picture. Let us pay attention to the part of the precipitation field located in the eastern half-plane from the radar, since it is here that the storms of interest to us developed. The most powerful of them, producing hail of different intensity, are marked with circles with crossing. The progress of the parameters of individual storms are presented on the side panels.

In general, we can see a certain structure of the precipitation field, along the linear elements of which the most powerful convective storms are concentrated.

Several convective storms from the panels (S3, 6, 9, 17) could be classified as "single-cell" if we rely on the radar parameter ΔHZ, which shows us one cycle of the object's development, while others (S15, 22) are classified as multi-cell.

As an example with which to review important details of the dynamics and kinematics, we turn to the horizontal cross-section S6 shown in panel (a). The structure of the radio echo: quasi-vertical and axisymmetric, the horizontal is quasi-symmetric circular. Everything corresponds to the ideal description of a "single-cell" storm [3]. The time course of the ΔHZ parameter, which is responsible, among other things, for the processes of hail formation and fallout (note especially the course of the ΔH55 parameter), indicates to us, together with the parameters of the vertical structure of the radio echo, the beginning of hail fallout at about 13:52. The inset fragment (b) shows two clear almost separate spots of hail falling, which tells us about two convective cells in this storm. We observe the same pattern in other storms.

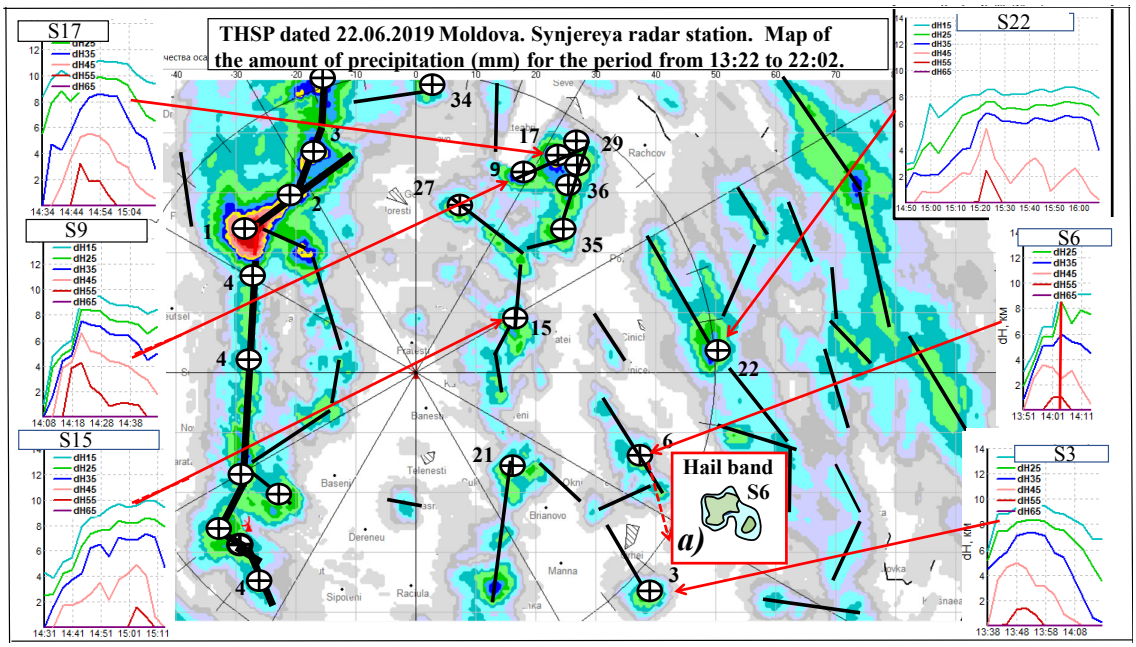

Figure 27. THSP precipitation map of 22.06.2019 in Moldova from 13:22 to 22:02. Cross-hatched circles show the position of individual convective storms. The black lines depict the facets of the MSCC. The panels on the left and right show the course of the *Δ*HZ parameters of the individual storms. Box a) shows two hail spots in the hail band S6 structure. The red vertical bar in the S6 panel corresponds to the time of hail fall beginning at 14:03.

The pattern of storms development in different directions with different velocities is quite similar to the "chaos" discussed in references [3,79], but the fact that the development of these storms is directed along linear fragments of structures or they are concentrated in the area of nodes speaks not of "chaos" but of regularity. Recall that the terrain over which the convective storms developed is practically flat, with height differences of no more than 100–150 metres, which cannot significantly affect their dynamics and kinematics.

Thus, having analysed all dynamical and kinematic parameters, we did not detect "single-cell" convective storms in this TSHP. Note that in our long-term practical work we have never managed to detect "single-cell" convective objects.

In summary, we can state that those objects that many authors call "single-cell convective storms", in particular, Chisholm et al. [24], and Abshaev "convective cells" [3], are in fact not such and consist of many small cells (updrafts flows), which are not distinguished by radar. This means that the "single-cell" storms can be classified as multicell storms with "weak evolution" in the same way as the multicell storms and all supercell storms in Foot and Frank [26] were divided into storms with "weak" and "strong" evolution.

Vasiloff et al. [31], observing the processes of transition of multicellular storms into supercellular storms and vice versa, consider that the structure of these two types of storms is almost identical and can be considered as a certain "continuum". In Section I, we have shown that the shape of the hail bands clearly shows hail falling simultaneously from several cells of a supercell storm. This means that the supercell is also, in fact, a multicell storm with weak evolution.

Summarizing, it can be stated that multicellularity is the only form of existence of vertical development clouds, and all these three groups of storms should be referred to the multicellular class by the main "genetic" feature of their similarity. For convenience and paying tribute to tradition, we can adopt the classification of Chisholm et al. [24], bearing in mind that the first group of storms—"single-cell" (if they exist), are essentially multicellular with "weak" evolution. Lemon [80], referring to Henderson [81], states that the latter has repeatedly observed flanking lines near "single-cell" storms.

The very facts suggest that these objects, called "single-cell" by the authors mentioned above, can only be multicell storms with "weak" evolution, and therefore evolve along the MSCC facets due to the merging of feeder cells with storms. As shown in our works [54,55,60,63], the convergence lines that form the image of meso-β-scale polygonal structures visible in the precipitation field are located at some angles to each other. The "chaotic" occurrence and displacement of "single-cell" storms along these convergence lines makes these processes explainable and most predictable, emphasizing the multicellularity of "single-cell" storms.

6. Renewal Band (RB) in convective storms. Flanking Line (FL)

The development of convective storms is associated with the inflow of cloud resource into the storm system in the form of feeder cells, which usually form a kind of "ladder" 20–30 km long (Flanking Line) with increasing cloud height as they approach the radar body of the storm. As we have already mentioned, the direction of the Flanking Line coincides with the direction of the evolution vector $\overrightarrow{V_e}$. It is therefore important to compare the perceptions of researchers who have studied the correlation of elements of different types of convective storms. Studies of the dynamics and kinematics of multicell and supercell convective storms by Browning and Ludlam [19], were developed by Chisholm and Renick [24] and by Marwitz [11]. These works laid the foundation of modern concepts of the inner cell and flow structure of convective storms.

6.1 RB and FL studies in supercell storms based on data in Moldova and the North Caucasus

Figure 28 shows a fragment of TSHP in the North Caucasus, the synoptic and aerological context of which can be found in reference [44]. This was a powerful convective process, in which two

supercells were noted, producing hail paths of several hundred kilometers with a hail diameter of 5 and more centimeters, and in some places a tornado was noted. We touched upon some aspects of this process in this paper (Chapters 3.3 and 3.7), as well as in our works [2,4,5,61,63]. In this case, we are interested in the way in which one of the supercells, which was assigned the conditional number 2, was updated at the expense of feeder cells. At some moments, the renewal process was recorded by radar. The dynamics of these episodes consisted in the fact that the 1st FC strip was built along the vector of the leading flux, covering the updating edge of the supercell in a kind of semicircle. The process of "absorption" of the 1st FC line (radiolocationally it is seen as a flow of radio echo towards the south and a general delineation by large values of reflectivity isocontours of this 1st FC line) is followed by the manifestation of the 2nd FC line, etc. The vertical section through the feeder cells line adjacent to the radar body of the storm (section 5) shows the shape of this line in the form of a "ladder", the height of which increases from left to right, and the height of feeder cells and their power also increase from left to right.

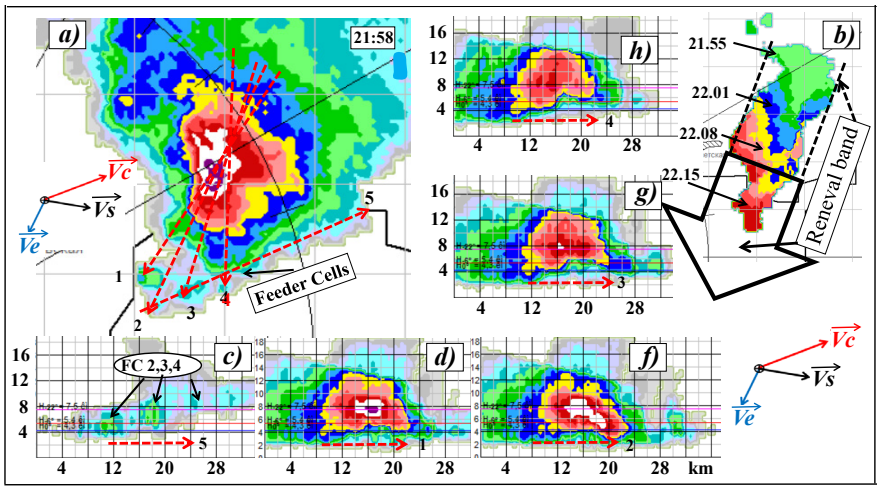

Figure 28. THSP of 08.19.2015 in the North Caucasus: (**a**) horizontal section of a supercell at an altitude of 5.4 km (T-6°); (**b**) renewal band; (**c, d, f, g, h**) vertical sections through feeder cells (red dotted arrows); vertical section numbers are indicated by numbers from 1 to 5. Scale grid on a 10 × 10 km horizontal cross-section.

Source: Livshits, et al [2,4].

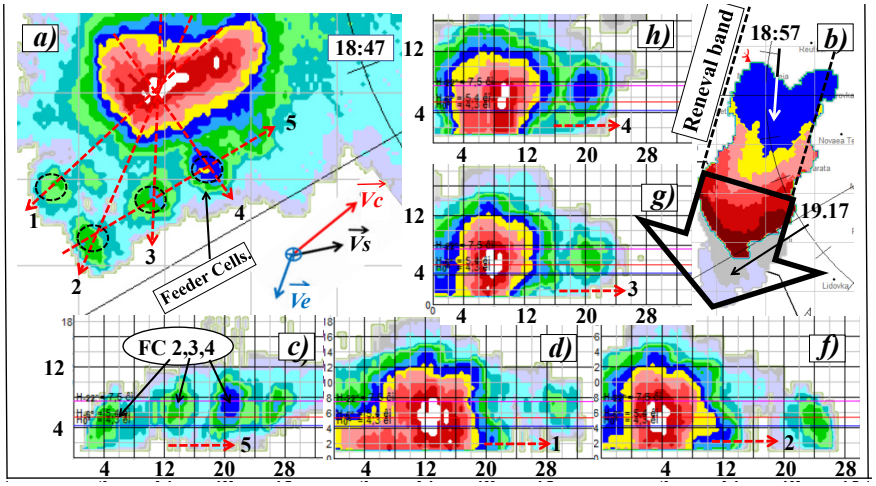

Figure 29. THSP of 18.06. 2016 in Moldova. All designations are similar to **Figure 28**.

Source: Livshits, et al [2,4].

We see exactly the same picture of supercell renewal in **Figure 29**, reflecting a similar situation in the TSHP of 18.06.2016 in Moldova (the aerosynoptic context of this supercell process is given in [2,3,4,55]), only the manifestation of the supercell renewal process here looks even more convincing.

It is important to note that the ratio of the driving vectors ($\overrightarrow{V_c}$, $\overrightarrow{V_s}$ and $\overrightarrow{V_e}$) are also identical: the overall orientation of the 1st FC line is almost the same as the direction of the leading flow vector ($\overrightarrow{V_c}$ and $\overrightarrow{V_e}$ indicates the general direction of the storm update. It is noticeable (**Figure 28b and 29b**) that the update process in the LCS manifests itself as a band with a width comparable to that of a radio echo with Z ≥ 45 dBZ, and the direction of this band coincides with the update vector ($\overrightarrow{V_e}$). We call this band the "renewal band" because new FCs "feeding" the storm appear within it. The FCs in the direction of storm renewal also line up in the form of a "ladder".

The striking similarity of supercell renewal processes in different regions (North Caucasus and Moldova) convinces us that it is not accidental, but regular and allows to hypothesise a "fine structure" of the renewal band, which will be discussed in Chapter 6.5.

6.2 RB and FL studies in multicell storms based on data in Moldova

Figure 30 presents two examples of multicell storm renewals in Moldova. Note that TSHP of 05.08.2014 developed in the slow-moving troposphere with wind shear in height significantly less than 1 m/sec/km, while THSP of 02.08.2021—in the fast-moving troposphere (the leading flow reached 17.5 m/sec with a total shear up to 2 m/sec/km). On the horizontal and vertical sections in both cases, the field of FCs was clearly visible, the first row of which covered the renewal part of the radio echo in the form of a semicircle. The repetition of the renewal cycles that retained some uniformity at different tropospheric velocities and wind shear is shown by the renewal band (broad arrow in panels (a) and (d), respectively). These and other relatively few facts (meaning the possibility of FC detection by radar) allowed us to hypothesize the cell structure of the update band, which will be discussed in Chapter 6.5.

6.3 Classical representations

In order to compare different ideas about the relationship between the FL and radar positions of the

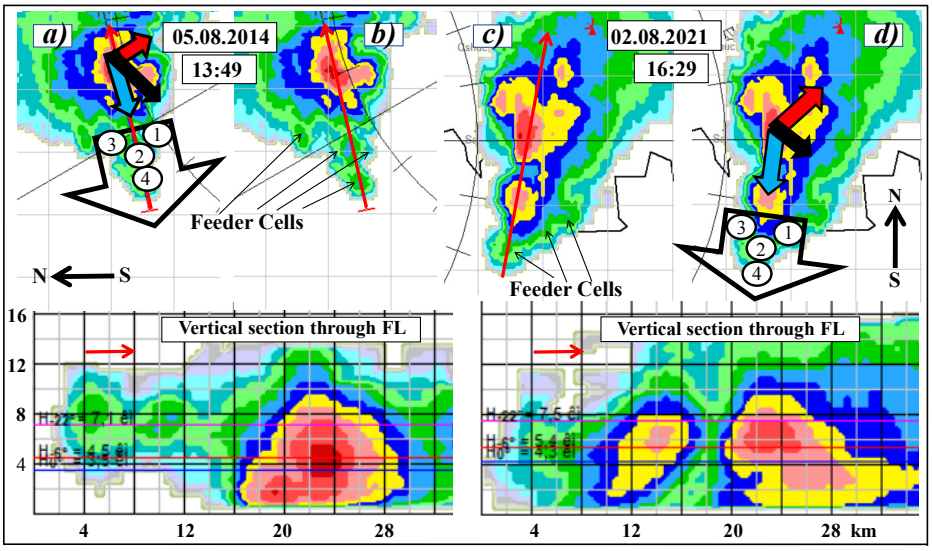

Figure 30. Structure of multicellular storm renewal bands in Moldova: (**a, b**) TSHP from 05.08.2014; (**c, d**) TSHP from 02.08.2021. The motion vectors for each of the storms are shown by vectors of different colours: red—$\overrightarrow{V_c}$ (vector of leading flow), black—$\overrightarrow{V_s}$, blue—$\overrightarrow{V_e}$.

Source: Livshits, et al [2,63].

storm body in different types of convective storms, we have analysed many comprehensive studies. In particular, we analysed in detail: the supercell storm Fleming storm (Browning et al. [21]), Acme storm (Krauss et al. [42]); the multicell storm Raymer storm (Browning et al. [82], Chalon et al. [22]); and a "hybrid" storm that combined features of both multicell and supercell storms (Hoeller et al. [83]). **Figure 31** shows the location of the radar body and FL for different supercell types: a) low precipitation (LP) supercell, (b)—classical (CS), (c) heavy precipitation (HP) supercell [30]. Panel (d) shows the position of the LFO relative to the multicell storm [84]. These schemes are the result of summarising and combining data from aircraft, satellite imagery, visual and radar observations.

Common for almost all of these storms is that *FL is oriented perpendicular to the direction of storm moving* (on the panels this direction is indicated as a white vector). The direction of storm moving coincides with the direction of the weak radio echo region (in the Russian interpretation - the direction of the radio echo canopy) relative to the main precipitation area, i.e. relative to the precipitation centroid. The Raymer storm example [22,82] seemed to be out of this picture, since the vectors $\overrightarrow{V_e}$ and $\overrightarrow{V_s}$ coincided. This was because the new cells in this storm were not formed in the usual way—ahead of the course of the storm. In Chapter 3.6, we showed that such storms are relatively rare and their recurrence in Moldova, the North Caucasus, and southern Brazil does not exceed 10%. At the same time, it should be noted that such collisions belong exclusively to multicell storms, which is confirmed by the analysis of the extensive world literature and confirms the main conclusion: the FL for storms of all types is always oriented along the evolution vector—$\overrightarrow{V_e}$.

6.4 Representations of the Russian school

Russian technology of anti-hail service (RT AHS) is based on the concept of acceleration of precipitation formation due to AgI impact on the first ones from the radar body of the storm FC. Flanking Line is assumed to be an extension of the radio echo canopy.

Figure 32 shows the scheme of the supercell according to Abshaev [62]. Externally, it looks the same as in foreign researchers [24,30], but one important detail is very different: the location of the Flanking Line (in the author [62] it is called Leading Clouds) is in the extension of the radio echo canopy.

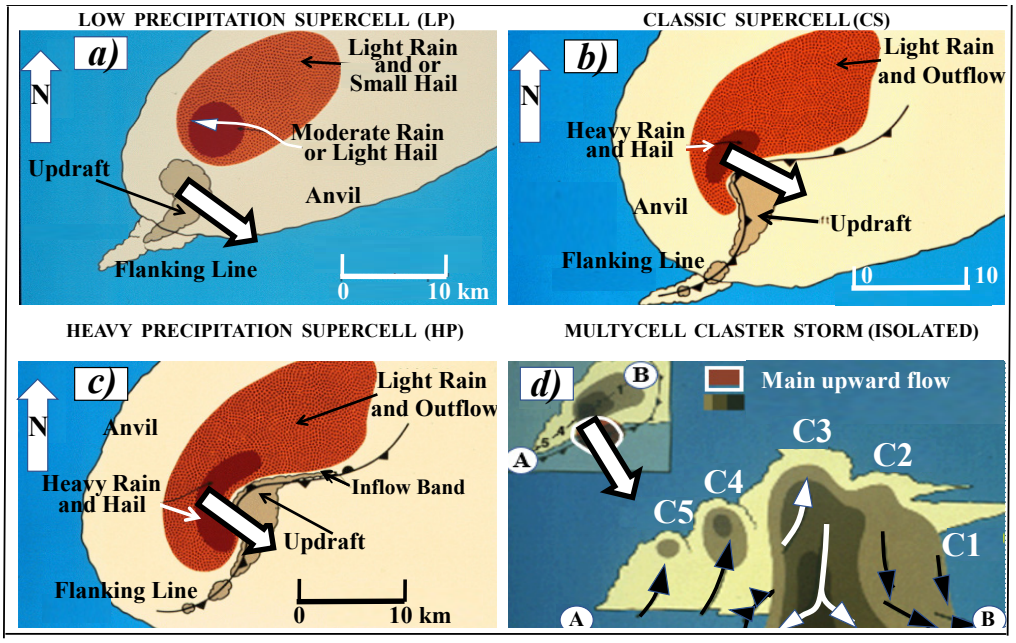

Figure 31. Stylised structure of supercell (**a, b, c**) and multicell storms (**d**). White arrow—direction of storm moving.

Source: Moller, et al [30,84].

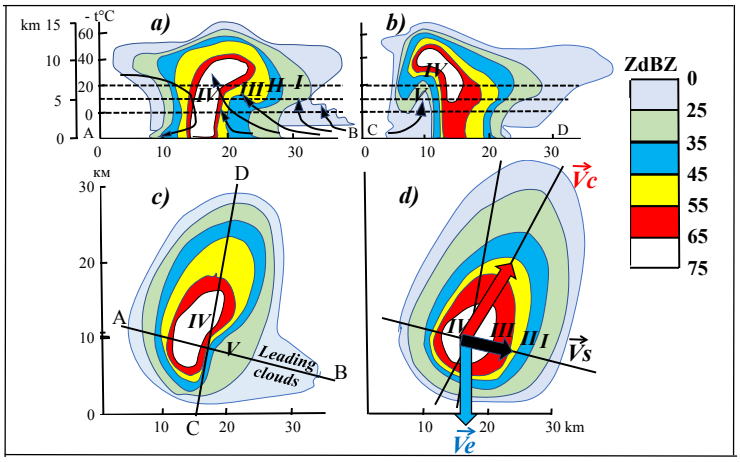

Figure 32. Russian scheme of a supercell with hail based on radar observations: (a)—vertical profile AB (in the direction of thunderstorm movement), (b)—vertical profile along CD (perpendicular to thunderstorm movement), (c)—horizontal profile at an altitude of 5 km (T = –6°C), (d)—horizontal profile at an altitude of 6 km (T = –12°C); I—the area of creation of conditions for hail formation, Il - hail nucleation area., Ill—area of hail growth, IV - area of maximum hail and V—strong updraft area.

Source: Abshaev, et al [62].

The literature analysis as well as our studies (Section 1) have shown that the occurrence of FC ahead along the storm track, i.e., in the canopy direction, is a very rare phenomenon, the recurrence of which is no more than 10% and refers exclusively to multicell storms. Supercells with renewals ahead of the storm have not been reported in the world literature.

Thus, there is a significant discrepancy between the two schools of thought about the mutual location of the LFO and the radar body of storms. The Flanking Line direction according to foreign (and our) ideas coincides with the direction of the evolution vector and differs from the Flanking Line direction according to Russian ideas by ≈ 90° to the right (left). In our opinion, such representations of the Russian school are speculative, since no airplane methods were used in storm studies, which allow us to compare visual and radar pictures. These differences also lead to the fact that the seeding sites are also different.

In Chapters 6.1 and 6.2, we considered the renewal process of supercell and multicell storms on the examples of the North Caucasus and Moldova. It was emphasised that the striking similarity of the renewal processes in the two supercells from different regions is not accidental, but natural. The renewal of two multicell storms in the slow-moving (at wind shear less than 1m/sec/m) and in the fast-moving troposphere (at wind shear greater than 2 m/sec/m) is also quite similar.

Based on these facts and rather disparate but important information from the literature, we present the author's view of the fine structure of the renewal band (RB) in **Figure 33**.

Panel a) shows the generalised RB structure for multicell storms in the form of a triangle whose base rests on the renewal part of the storm. The orientation of the long axis of the triangle is along the evolution vector. The storm canopy, whose orientation coincides with the direction of its displacement, makes an angle ≈ 90° with the evolution vector.

In panel c), the RB structure for the supercell storm looks like a "comma" whose arc faces the direction of the storm's displacement. This is due to the presence of a mesocyclone in the supercells, whose rotation causes a "deformation" of the RB, and its orientation generally corresponds to the evolution vector. The angle between the storm trajectory and the RB direction is also equal to ≈ 90°.

Panel b) shows the structure of the RB supercell, which, as we showed in reference [2] when analysing the Fleming storm, also contained FCs. They were lined up in an unusual way—in the form of an arc, tightly "pinned" to the radar body of the storm. A gust front in such cases should move at a rate of renewal of storm.

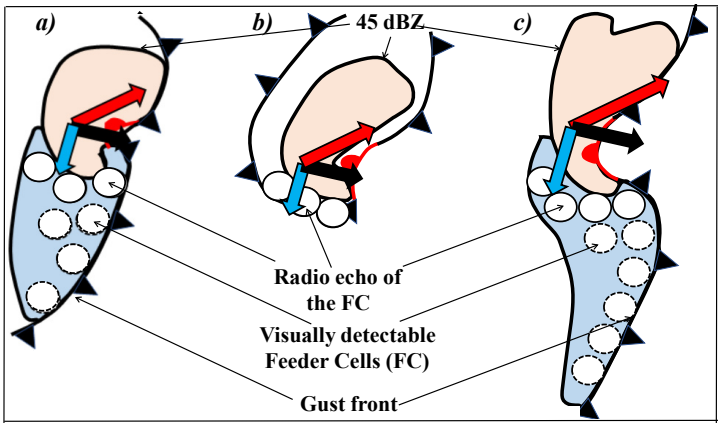

Figure 33. Renewal band (RB) structure: (**a**) RB as "triangle" in multicell storms: (**b**) with RB as "arc" in supercells; (**c**) with RB as "comma" in supercells. Gust fronts in the corresponding parts are labelled with black triangles (cold) and red semicircles (warm) (**a**) and (**c**)). Motion vectors: red—$\overrightarrow{V_c}$, black—$\overrightarrow{V_s}$, blue—$\overrightarrow{V_e}$.

Source: Livshits, et al [2].

To explain this phenomenon, we propose a hypothesis suggesting that the renewal process is concentrated in the form of a narrow arc-shaped band. This band cannot unfold, as it is prevented by the gust front "enclosing" all the renewal processes behind the front of the supercell cold pool. Normally in supercells, the gust front "unfolds" as a Flanking Line oriented perpendicular to the storm displacement vector, but in this case it "roll up" as an arc. The presence of the Vertical Flanking Line, which has been repeatedly observed by Bluestein [78], may have occurred in this particular case.

The hypotheses expressed here regarding the structure of the renewal band for different types of storms need to be confirmed by in-situ observations. Nevertheless, the first step we have taken in this direction gives an idea of the possible mechanisms of the renewal band organisation and contributes to a deeper understanding of the physics of these processes.

7. Conclusions

The article outlines the results of our studies of the last few years, for which we also involved materials of foreign and Russian authors. These studies are based on the hypothesis of translation of cellular convection (of the Rayleigh-Benard convection type) from the surface layer to the upper layers of the troposphere.

The dynamics and kinematics of convective storms are sufficiently well studied in the Eulerian coordinate system. However, the presence of tropospheric displacement under the action of winds does not allow us to obtain an adequate picture of the development of convective structures TSHP in this coordinate system

The verification of the above hypothesis required a different approach. And such an approach was found: the Lagrange principle, which consists in that the observer is "placed" in the centre of this coordinate system and moves together with it against the leading flow and with the velocity of the leading flow.

This approach allows us to detect and trace the dynamics of mesoscale cellular convection, which is found to have a net structure. Precisely as a result of the Lagrangian approach, it was possible to establish that the manifestation of all convective phenomena is determined by the configuration and dynamics of the meso-β-scale structure of the TSHP, and the number of different variants of the manifestation of convective phenomena is reduced by more than an order of magnitude compared to the Euler coordinate system.

It was found that the orientation of the canopies of radio echoes of convective storms practically coincides with the trajectories of storm displacement.

It was shown that the renewal of all types of convective storms occurs in the renewal band in the direction of the evolution vector due to feeder cells.

In the most powerful hail storms with a stationary canopy of radio echoes, the evolution vector deviates from the storm displacement vector by 80°–135°.

The internal structure of renewal bands, consisting of feeder cells that line up in certain structures, was shown. These internal structures of renewal bands depend on the type of storm, and their formation is related to the peculiarities of airflow interaction with the MSCC structure in the storm system.

As a result of a detailed analysis of one of the supercell storms (Fleming storm), a hypothesis is formulated to explain the Flanking Line configuration in the form of a vertical wall arranged in an arc near the radar body of the supercell storm.

It is shown that the orientation of the hail bands indicates the direction of the convective storm development, which coincides with the evolution vector, which can serve as an indicator of the Flanking Line orientation, and the elongation of hail bands with lengths greater than 5–6 km also indicates the multicellularity of even supercells.

It was found that the mutual orientation of the anvils of powerful convective storms can serve as an indicator of their kinematic characteristics. Two mnemonic rules were proposed that allow us to determine left- or right-moving storms and the convergence or divergence of their trajectories from the simultaneous pattern of two storm anvil orientation and their mutual location.

Based on radar observations of the unique displacement of a multi-cell storm in the North Caucasus, we derive a scheme of the structure of a cold front of the 2nd kind and formulate a hypothesis explaining this structure.

We study in detail the splitting of convective storms, which we link to the processes occurring in the MSCC nodes: the deviation of the MSCC edges from the nodal region leads to the renewal of the storm on different flanks and its subsequent separation.

Three new convective phenomena are found, which complete the known classification of the types of convective storm development at MSCC elements:

- splitting of a multi-cell convective storm in a low-moving and low-shear troposphere, in which one storm moves along its trajectory, while the second storm remains in place after splitting (the "droplet splitting" phenomenon);

- the development of a convective "nodal" storm that is updated from the inner parts of the MSCC; a hypothesis has been proposed to explain this unique phenomenon;

- "double" convective "merger-splitting" phenomenon.

The process of merging of convective storms has been studied. An algorithm is proposed that allowed us to distinguish between two fundamentally different phenomena: the merger of convective storms with feeder cells and the merger of storms themselves.

A typification of the consequences of the mergers was carried out. In contrast to the generally accepted opinion that almost all storm mergers lead to their intensification and development, we found that 2/3 of all hail storms dissipate after merging, and only 1/3 develop.

It was hypothesised that there is a mechanism of merging of convective storms, which is associated with a certain configuration of MSCC facets and nodes. The main "actors" of the merger process are Flanking Lines, whose mutual orientation affects both the speed and the consequences of mergers.

The existence of so-called "single-cell convective storms" is considered. It is concluded that "single-cell convective storms" are the same as multicell storms, only with weak evolution. In contrast to the view of some researchers of single-cell storms that their behaviour is "chaotic" and "unpredictable", we consider their behavior to be completely natural and predictable. We also conclude that all types of convective storms constitute the class of multicell storms, since the only form of existence of convective storms is their multicellularity.

The obtained results are applicable in the practice of modifying convective clouds, in the system of storm warning of the population, for rescue services and other state organisations.

We associate the further prospect of research with the study of processes occurring at the junction of

two spaces—Eulerian and Lagrangian. This will help to discover more reliable predictors for ultra-short-term forecasts of the dynamics and kinematics of convective storms of any type and related hazardous weather phenomena.

Author Contributions

Both authors contributed equally to this article.

Conflict of Interest

There is no conflict of interest.

Data Availability Statement

Data were provided by the Anti-hail services of the Republic of Moldova and the North Caucasus Anti-hail service of the Russian Federation.

Funding

This research received no external funding.

Acknowledgements

The materials of radar observations in Moldova were provided by the head of the anti-hail service Garaba I.A., in the North Caucasus—by Dr. Abshaev A.M. The authors are grateful to Prof. Shchukin G.G. and Dr. Korneev V.P. for active and useful participation in the discussion of the results.

References

[1] Starostin, A.N., Livshits, E.M., Shvetsov, V.S. 1983. Mesoscale structure of radio echo fields of convective clouds in Moldova. Meteorology and Hydrology.10, 55–59. [In Russian].

[2] Livshits, E.M., 2023. Dynamics and kinematics of convective storms on elements of meso-β-scale convective structures. M. 324. [In Russian].

[3] Abshaev, M.T., Abshaev, A.M., Barekova, M.V., Malkarova, A.M. 2014. Guidelines for organizing and conducting anti-hail operations. Nalchik. 500. [In Russian].

[4] Livshits, E.M., Petrov, V.I. 2021. Radar detection of the location of the feeding cloud line. Part I. Main motion vectors and their relation in severe hail storms. Proceedings of the All-Russian Open Conference on FO and AB on Hydrometeorological Processes. Nalchik. 192–198. [In Russian].

[5] Livshits, E.M., Petrov, V.I., 2021. Radar detection of the location of the feeding cloud line. Part II. Results of the study. Proceedings of the All-Russian Open Conference on FC and AI on Hydrometeorological Processes. Nalchik. 198–204. [In Russian].

[6] Hitschfeld, W., 1960. The motion and erosion of convective storms in severe vertical wind shear. Journal of the Atmospheric Sciences. 17(3), 270–282.
DOI: https://doi.org/10.1175/1520-0469(1960)017%3C0270:TMAEOC%3E2.0.CO;2

[7] Newton, C.W., Fankhauser, J.C., 1964. On the movements of convective storms, with emphasis on size discrimination in relation to water budget requirements. Journal of Applied Meteorology and Climatology. 3(6), 651–668.
DOI: https://doi.org/10.1175/1520-0450(1964)003%3C0651:OTMOCS%3E2.0.CO;2

[8] Fujita, T., Grandoso, H., 1968. Split of a thunderstorm into anticyclonic and cyclonic storms and their motion as determined from numerical model experiments. Journal of the Atmospheric Sciences. 25, 416–439.
DOI: https://doi.org/10.1175/1520-0469(1968)025%3C0416:SOATIA%3E2.0.CO;2

[9] Charba, J., Sasaki, Y., 197I. Structure and movement of the severe thunderstorms of 3 April 1964 as revealed from radar and surface mesonetwork data analysis. Journal of the Meteorological Society of Japan. Ser. II. 49(3), 191–214.
DOI: https://doi.org/10.2151/JMSJ1965.49.3_191

[10] Haglund, G.T., 1969. A study of a severe local storm of 16 April 1967. ESSA Technical Memorandum. ERLTM-NSSL 44. National Severe

Storms Laboratory: Norman, OK. pp. 54.

[11] Marwitz, J.D., 1972. The structure and motion of severe hailstorms. Part I: Supercell storms. Journal of Applied Meteorology and Climatology. 11(1),166–179.
DOI: https://doi.org/10.1175/1520-0450(1972)011%3C0166:TSAMOS%3E2.0.CO;2

[12] Burgess, D.W., Lemon, L.R., Achtemeier, G.L., 1976. Severe storm splitting and left-moving storm structure. The Union City Tornado of 24 May 1973, NOAA Technical Memorandum. ERL NSSL-80, National Severe Storms Laboratory: Norman, OK. pp. 53–66.

[13] Bluestein, H.B., Sohl, C.J., 1979. Some observations of a splitting severe thunderstorm. Monthly Weather Review. 107(7), 861–873.
DOI: https://doi.org/10.1175/1520-0493(1979)107<0861:SOOASS>2.0.CO;2

[14] Lemon, L.R., Burgess, D.W., 1980. Magnitude and implications of high speed outflow at severe storm summits. Preprints, 19th Conf. on Radar Meteorology, Miami Beach, FL, Amer. Meteor. Soc. 364–368.

[15] Kubesh, R.J., Musil, D.J., Farley, R.D., et al., 1988. The 1 August 1981 CCOPE storm: observations and modeling results. Journal of Applied Meteorology and Climatology. 27(3), 216–243.
DOI: https://doi.org/10.1175/1520-0450(1988)027%3C0216:TAMSOA%3E2.0.CO;2

[16] Brown, R.A., 1992. Initiation and evolution of updraft rotation within an incipient supercell thunderstorm. Journal of the Atmospheric Sciences. 49(21), 1997–2031.
DOI: https://doi.org/10.1175/1520-0469(1992)049<1997:IAEOUR>2.0.CO;2

[17] Burgess, D.W., Curran, E.B., 1985. The relationship of storm type to environment in Oklahoma on 26 April 1984. Preprints, 14th Conf. on Severe Local Storms, Indianapolis, IN, Amer. Meteor. Soc. 208–211.

[18] Conway, J.W., Weisman, M.L., 1988. An investigation into the splitting and propagation of the 13 June 1984 Denver hailstorms. Preprints, 15th Conf. on Severe Locof Storms, Baltimore, MD, Amer. Meteor. Soc. 276–279.

[19] Browning, K.A., Ludlam, F. H., 1960. Radar analysis of a hailstorm. Tech. Note No. 5. Dept. of Meteorology. Imperial College. London. 106.

[20] Bluestein, H.B., Parker, S.S., 1993. Modes of isolated, severe convective storm formation along the dry line. Monthly Weather Review. 121(5), 1354–1372.
DOI: https://doi.org/10.1175/1520-0493(1993)121<1354:MOISCS>2.0.CO;2

[21] Browning, K.A., Foote, G.B., 1976. Airflow and hail growth in supercell storms and some umplications for hail suppression. Quarterly Journal of the Royal Meteorological Society, 102(433), 499–533.
DOI: https://doi.org/10.1002/QJ.49710243303

[22] Chalon, J.-P., Fankhauser, J.C., Eccles, P.J. 1976. Structure of an evolving hailstorm. Part I: general characteristic and cellular structure. Monthly Weather Review. 104(5), 564–575.
DOI: https://doi.org/10.1175/1520-0493(1976)104<0564:SOAEHP>2.0.CO;2

[23] Chisholm, A.J., 1973. Alberta Hailstorms Part I: Radar case studies and airflow models. Alberta Hailstorms. Meteorological Monographs. American Meteorological Society: Boston, MA. pp. 1–36.
DOI: https://doi.org/10.1007/978-1-935704-32-4

[24] Chisholm, A.J., Renick, J.H., 1972. The kinematics of multicell and supercell Alberta hailstorms. Alberta Hail Studies 1972. Research Council of Alberta. Hail Studies Report. 72–2, 24 –31.

[25] Fankhauser, J.C., 1982. Hailstorms of the Central High Plains. Vol. 2. Part I: 22 June 1976 case study—a complex multicellular hail and rainstorm. Chap. 13: Large-scale influences, radar echo structure and mesoscale circulations. C. Knight. P. Squires. Eds. Colorado Assoc. University Press.

[26] Foot, G.B., Frank, H.W., 1983. Case study of a hailstorm in Colorado. Part III: Airflow from triple-doppler measurements. Journal of the At-

mospheric Sciences. 40(3), 686–707.
DOI: https://doi.org/10.1175/1520-0469(1983)040<0686:CSOAHI>2.0.CO;2

[27] Westcott, N.E., Kennedy, P.C., 1989. Cell development and merger in an Illinois thunderstorm observed by doppler radar. Journal of the Atmospheric Sciences. 46(1), 117–131.
DOI: https://doi.org/10.1175/1520-0469(1989)046<0117:CDAMIA>2.0.CO;2

[28] Klose, B., Klose, H., 2015. Meteorologie. Eine interdisziplinaere Einfuerung in die Physik der Atmosphaere. Springer Spektrum Berlin: Heidelberg.
DOI: https://doi.org/10.1007/978-3-662-43578-6

[29] Lemon, L.R., Doswell, C.A. III., 1979. Severe thunderstorm evolution and mesocyclone structure as related to tornadogenesis. Monthly Weather Review. 107 (9), 1184–1197.
DOI: https://doi.org/10.1175/1520-0493(1979)107<1184:STEAMS>2.0.CO;2

[30] Moller, A.R., Doswell III C.A., Foster, M.P., et al., 1994. The operational recognition of supercell thunderstorm environments and storm structures. Weather and Forecasting. 9(3), 327–347.
DOI: https://doi.org/10.1175/1520-0434(1994)009<0327:TOROST>2.0.CO;2

[31] Vasiloff, S.V., Brandes, E.A., Davies-Jones, R.P., 1986. An investigation of the transition from multicell to supercell storms. Journal of Climate and applied Meteorology. 25(7), 1022–1036.
DOI: https://doi.org/10.1175/1520-0450(1986)025<1022:AIOTTF>2.0.CO;2

[32] Davies-Jones, R., Doswell III, C.A., Brooks H.E., 1994. Comments on "initiation and evolution of updraft rotation within an incipient supercell thunderstorm". Journal of the Atmospheric Sciences. 51(2), 326–331.
DOI: https://doi.org/10.1175/1520-0469(1994)051<0326:COAEOU>2.0.CO;2

[33] Starostin A., Abdoullaev S., Nunes A.B., 2000. Storm evolution in nonlinear mesoscale convective systems. XI Brazilian Meteorological Congress.1990–1995.[In Portuguese]

[34] Heymsfield, A. J., Jameson, A.R., Frank, H.W., 1980. Hail growth mechanisms in a Colorado storm. Part II: Hail formation processes. Journal of the Atmospheric Sciences. 37(8), 1779–1807.
DOI: https://doi.org/10.1175/1520-0469(1980)037<1779:HGMIAC>2.0.CO;2

[35] Tessendorf ,S.A., Miller, L.J., Wiens, K.C., et al., 2005. The 29 June 2000 supercell observed during STEPS. Part I: Kinematics and Microphysics. Journal of the Atmospheric Sciences. 62(12), 4127–4150.
DOI: https://doi.org/10.1175/JAS3585.1

[36] Cheng, L., Rogers, D.C., 1988. Hailfalls and hailstorm feeder clouds—an alberta case study. Journal of the Atmospheric Sciences. 45(23), 3533–3545.
DOI: https://doi.org/10.1175/1520-0469(1988)045%3C3533:HAHFCA%3E2.0.CO;2

[37] Gilbert, D.B., Boe, B.A., Krauss ,T.W., 2016. Twenty seasons of airborne hail suppression in Alberta, Canada. The Journal of Weather Modification. 48(1), 68–93.
DOI: https://doi.org/10.54782/jwm.v48i1.551

[38] Mazur, R.J., Weaver, J.F., Van der Haar, T.H., 2007. Observations of inflow feeder clouds and their relation to severe thunderstorm. 22 Conference on Weath. Analysis and Forecast. 18.

[39] Levizzani, V., Amorati, R., Meneguzzo, F., 2002. A review of satellite based rainfall estimation methods. Environmental Science, Geography. 1–66.
DOI: https://www.researchgate.net/publication/252272255

[40] Mecikalski, J.R., Williams, J.K., Jewett, C.P., et al., 2015. Probabilistic 0–1-h convective initiation nowcasts that combine geostationary satellite observations and numerical weather prediction model data. Journal of Applied Meteorology and Climatology. 54(5), 1039–1059.
DOI: https://doi.org/10.1175/JAMC-D-14-0129.1

[41] Krauss, T.W., Renick, J., 2021. The New Alberta Hail Suppression Project. The Journal of

Weather Modification. 29(1), 100–105.
DOI: https://doi.org/10.54782/jwm.v29i1.474

[42] Krauss, T.W., Marwitz, J.D., 1984. Precipitation process within an alberta supercell hailstorm. Journal of the Atmospheric Sciences. 41(6), 1025–1035.
DOI: https://doi.org/10.1175/1520-0469(1984)041<1025:PPWAAS>2.0.CO;2

[43] Abshaev, M.T., Abshaev, A.M., Malkarova A.M., et al., 2022. Protection of agricultural plants from hailstorms in the North Caucasus. Meteorology and Hydrology. 7, 11–27. [In Russian].

[44] Abshaev, M.; Abshaev, A.; Sinkevich, A.; et al., 2019. Characteristics of the Supercell Cb Thunderstorm and Electrical Discharges on 19 August 2015, North Caucasus: A Case Study. Preprints. 2019120033.
DOI: https://doi.org/10.20944/preprints201912.0033.v1

[45] Skamarock, W.C., Klemp, J.B., Dudhia, J., et al., 2021. A Description of the Advanced Research WRF Model Version 4.3 (No. NCAR/TN-556+STR).
DOI: https://doi.org/10.5065/1dfh-6p97

[46] Hersbach, H., Bell, B., Berrisford P., et al., 2020. The ERA5 global reanalysis. Quarterly Journal of the Royal Meteorological Society. 146, 1999–2049.
DOI: https://doi.org/10.1002/qj.3803

[47] Lindsey, D.T, Bunkers, M.J., 2005. Observations of a severe, left-moving supercell on 4 May 2003. Weather and Forecasting. 20(1), 15–22.
DOI: https://doi.org/10.1175/WAF-830.1

[48] Setvak, M., Bedka, K., Lindsey, D.T., et al., 2013. A-train observations of deep convective storm tops. Atmospheric Research. 123, 229–248.
DOI: https://doi.org/10.1016/j.atmosres.2012.06.020

[49] Minnachmetov, R.M., Starostin, A.N., 1989. Radar observations of cell convection in the atmospheric boundary layer. Active impact on atmospheric processes in Moldova. Kishinev "Shtiyintsa". 55–61. [In Russian].

[50] Banghoff, J.R., Sorber, J.D., Stensrud, D.J., et al., 2019. A 10-Year warm-season climatology of horisontal convective rolls and cellular convection in Central Oklahoma. Monthly Weather Review. 148(1). 21–42.
DOI: https://doi.org/10.1175/MWR-D-19-0136.1

[51] Minnachmetov, R.M., Starostin, A.N., 1986. Spatial and temporal structure of the thunderstorm process on June 28, 1982. Active influence on the atmospheric processes in Moldova. Kishinev. 29–43. [In Russian].

[52] Starostin, A.N., 1992. Classification of types of cumulonimbus cloud evolution. Active influence on atmospheric processes in Moldova. Kishinev. 58–74. [In Russian].

[53] Livshits, E.M., Petrov, V.I., 2021. Splitting of convective storms. Part II. organization of the mesoscale structure of the thunderstorm process. Hydrometeorology and Ecology. 66, 648–670. [In Russian].
DOI: https://doi.org/10.33933/2713-3001-2021-65-648-670

[54] Livshits, E.M., Petrov, V.I., 2022. Merging of convective storms and their typing. Hydrometeorology and Ecology. 69, 620–643. [In Russian].
DOI: https://doi.org/10.33933/2713-3001-2022-69-620-643

[55] Livshits, E.M., Petrov, V.I., 2023. A special type of multicell storms developing in the nodes of meso-β-scale convective structures. Scientific and Practical Journal "Notes of a Scientist". 6, 175–189. [In Russian].

[56] Stull, R., 2016. Practical Meteorology: An Algebra-based Survey of Atmosphere Science. Vancouver, Canada: The University of British Columbia. 924.

[57] Charba, J., Sasaki, Y., 1971. Structure and movement of the severe thunderstorms of 3 April 1964 as revealed from radar and surface mesonet work data analysis. Journal of the Meteorological Society of Japan. Ser. II. 49(3),

191–214.
DOI: https://doi.org/10.2151/jmsj1965.49.3_191

[58] Wang, C.-C., Chen T.-J. G., Yang, S.-C., et al., 2009. Wintertime supercell thunderstorms in a subtropical environment: numerical simulation. Monthly Weather Review. 137(7), 2175–2202.
DOI: https://doi.org/10.1175/2008MWR2616.1

[59] Bocheva, L., Dimitrova, T., Penchev, R., et al., 2018. Severe convective supercell outbreak over western Bulgaria on July 8, 2014. Quarterly Journal of the Hungarian Meteorological Service. 122(2), 101–216.
DOI: https://doi.org/10.28974/idojaras.2018.2.5

[60] Livshits, E.M, Petrov, V.I., 2021. The splitting of convective storms. Part I. dynamics and kinematics. Journal of Hydrometeorology and Ecology. 65, 648–670. [In Russian].
DOI: https://doi.org/10.33933/2713-3001-2021-65-648-670

[61] Livshits, E.M., Petrov, V.I., 2023. To the question of wind shear with height and its influence on the dynamics and kinematics of convective storms. Scientific and Practical Journal "Science and Production". 2, 75–87. [In Russian].

[62] Abshaev, M.T., 1982. Structure and dynamics of development of thunderstorm-hail processes of the North Caucasus. Proc. VGI. 53, 6–22. [In Russian].

[63] Livshits, E.M., Petrov, V.I., 2023. Renewal Band Structure in Deep Convective Storms. Russian Meteorology and Hydrology. 48(8), 722–732.
DOI: https://doi.org/10.3103/S1068373923080101

[64] Westcott, N.E., 1994. Merging of convective clouds: Cloud initiation, bridging and subsequent growth. Monthly Weather Review. 122(5), 780–790.
DOI: https://doi.org/10.1175/1520-0493(1994)122<0780:MOCCCI>2.0.CO;2

[65] Fu, D., Guo, X., 2011. Cloud-resolving simulation study on the merging processes and effects of topography and environmental winds. Journal of the Atmospheric Sciences. 69(4), 1232–1249.
DOI: https://doi.org/10.1175/JAS-D-11-049.1

[66] Tao, W.-K., Simpson, J., 1989. A further study of cumulus interactions and mergers: three-dimensional simulations with trajectory analyses. Journal of the Atmospheric Sciences. 46(19), 2974–3004.
DOI: https://doi.org/10.1175/1520-0469(1989)046<2974:AFSOCI>2.0.CO;2

[67] Lin, Y.-L., Joyce, L.E., 2001. A further study of the mechanisms of cell regeneration, propagation, and development within two-dimensional multicell storms. Journal of the Atmospheric Sciences. 58(20), 2957–2988.
DOI: https://doi.org/10.1175/1520-0469(2001)058<2957:AFSOTM>2.0.CO;2

[68] Lee, B.D., Jewett, B.F., Wilhelmson, R.B., 2006. The 19 April 1996 Illinois tornado outbreak. Part I: Cell evolution and supercell isolation. Weather Forecasting. 21(4), 433–448.
DOI: https://doi.org/10.1175/WAF944.1

[69] Carey, L.D., Petersen, W.A., Rutledge, S.A., 2003. Evolution of cloud-to-ground lightning and storm structure in the Spencer, South Dakota, tornadic supercell of 30 May 1998. Montly Weather Review. 131(8), 1811–1831.
DOI: https://doi.org/10.1175//2566.1

[70] Gauthier, M., Petersen, W.A., Carey, L., 2010. Cell mergers and their impact on cloud-to-ground lightning over the Houston area. Atmospheric Research. 96(4), 626–632.
DOI: https://doi.org/10.1016/j.atmosres.2010.02.010

[71] Lu, J., Qie, X., Jiang, R., 2021. Lightning activity during convective cell mergers in a squall line and corresponding dynamical and thermodynamical characteristics. Atmospheric Research. 256, 105555.
DOI: https://doi.org/10.1016/j.atmosres.2021.105555

[72] Sinkevich, A.A., Krauss, T.V., 2010. Impacts on clouds in Saudi Arabia, statistical evaluation of the results. Meteorology and Hydrology. 6, 26–37. [In Russian].

[73] Sinkevich, A.A., Dovgalyuk, Yu. A., Veremey,

N.E., et al., 2018. Convective cloud merger. St. Petersburg. Amirit Ltd. 280. [In Russian].

[74] Krauss, T.W., Sinkevich, A.A., Ghulam, A.S., 2011. Effects of feeder cloud merging on storm development in Saudi Arabia. Journal of King Abdulaziz University-Meteorology Environment and Arid Land Agriculture Sciences. 22(2), 23–39.

[75] Simpson, J., Keenan, T.D., Ferrier, B., et al., 1993. Cumulus mergers in the maritime continent region. Meteorology and Atmospheric Physics. 51, 73–99.
DOI: https://doi.org/10.1007/BF01080881

[76] Sinkevich, A., Krauss, T., 2014. Changes in thunderstorm characteristics due to feeder cloud merging. Atmospheric Research. 142, 124–132.
DOI: https://doi.org/10.1016/j.atmosres.2013.06.007

[77] Stalker, J.R., Knupp, K.R., 2003. Cell merger potential in multicell thunderstorms of weakly sheared environments: Cell separation distance versus planetary boundary layer depth. Monthly Weather Review. 131. P. 1678–1695.
DOI: https://doi.org/10.1175//2556.1

[78] Bluestein, H. B., 1986. Visual aspects of the flanking line in severe thunderstorms. Monthly Weather Review. 114 (4), 788–795.
DOI: https://doi.org/10.1175/1520-0493(1986)114<0788:VAOTFL>2.0.CO;2

[79] Appayeva Zh. Yu., Cherednik, E.A., 2018. Peculiarities of distribution of the main radar characteristics of single-cell hail clouds of the North Caucasus. Reports of the Third International Scientific Conference with elements of scientific school. Stavropol, 35–39. [In Russian].

[80] Lemon, L.R., 1976. The flanking line, a severe thunderstorm intensification source. Journal of the Atmospheric Sciences. 33(4), 686–694
DOI: https://doi.org/10.1175/1520-0469(1976)033<0686:TFLAST>2.0.CO;2

[81] Henderson, T.J., 1968. 6000 thunderstorms and what they indicate. Proc. Intern. Conf. Cloud Physics, Toronto. 555–558

[82] Browning, K.A., Fankhauser, J.C., Chalon, J.P., et al., 1976. Structure of an evolving hailstorm, part v; synthesis and implications for hail growth and hail suppression. Monthly Weather Review. 104(5), 603–610.
DOI: https://doi.org/10.1175/1520-0493(1976)104%3C0603:SOAEHP%3E2.0.CO;2

[83] Hoeller, H., Bring,i V.N., Hubbert, J., et al., 1994. Life cycle and precipitation formation in a hybrid-type hailstorm revealed by polarimetric and doppler radar measurements. Journal of the Atmospheric Sciences. 51 (17), 2500–2522.
DOI: https://doi.org/10.1175/1520-0469(1994)051<2500:LCAPFI>2.0.CO;2

[84] LaDue, J.G., LaDue, D.S., 2008. Convective Storm Classification: is it in Need of Change? Environmental Science. 1–10.